© 2022. Published by The Company of Biologists Ltd | Journal of Cell Science (2022) 135, jcs259825. doi:10.1242/jcs.259825

RESEARCH ARTICLE

Tandem C2 domains mediate dynamic organelle targeting of a DOCK family guanine nucleotide exchange factor

Eileen L. Mallery[1,*], Makoto Yanagisawa[1,*], Chunhua Zhang[1,2,‡], Youngwoo Lee[1,2], Linda M. Robles[3], Jose M. Alonso[3] and Daniel B. Szymanski[1,2,4,§]

ABSTRACT

Multicellular organisms use dedicator of cytokinesis (DOCK) family guanine nucleotide exchange factors (GEFs) to activate Rac/Rho-of-plants small GTPases and coordinate cell shape change. In developing tissues, DOCK signals integrate cell-cell interactions with cytoskeleton remodeling, and the GEFs cluster reversibly at specific organelle surfaces to orchestrate cytoskeletal reorganization. The domain organizations among DOCK orthologs are diverse, and the mechanisms of localization control are poorly understood. Here, we use combinations of transgene complementation and live-cell imaging assays to uncover an evolutionarily conserved and essential localization determinant in the DOCK-GEF named SPIKE1. The SPIKE1-DHR3 domain is sufficient for organelle association *in vivo*, and displays a complicated lipid-binding selectivity for both phospholipid head groups and fatty acid chain saturation. SPIKE1-DHR3 is predicted to adopt a C2-domain structure and functions as part of a tandem C2 array that enables reversible clustering at the cell apex. This work provides mechanistic insight into how DOCK GEFs sense compositional and biophysical membrane properties at the interface of two organelle systems.

KEY WORDS: DOCK, Rac/Rho-of-plants, Lipid binding, Organelle association, Small GTPases

INTRODUCTION

Guanine nucleotide exchange factors (GEFs) activate small GTPases by promoting guanosine diphosphate (GDP) dissociation and re-equilibration with the cellular pool of guanine nucleotides, which exist at high GTP:GDP ratios (Berken and Wittinghofer, 2008; Rossman et al., 2005; Schmidt and Hall, 2002). Rho/Rac GEFs function as part of a regulatory module that includes GTPases that accelerate the intrinsic rate of GTP hydrolysis, and guanine nucleotide dissociation factors that influence the subcellular partitioning of Rac between cytosolic and membrane-associated pools. Eukaryotic cells transiently concentrate components of this regulatory module at specialized cortical sites to couple conformational changes in Rac that occur upon GTP binding with the input-output behaviors of the signaling switch (Chiou et al., 2017; Denninger et al., 2019; Etienne-Manneville and Hall, 2002; Kost, 2008; Oda and Fukuda, 2012). An important challenge is to understand how membrane targeting of regulatory factors influences Rac signaling functions.

Part of the answer lies in Rac itself. Rac orthologs, in plants termed Rho-of-plants (ROP) proteins, contain acylation sites and patches of positively charged amino acids in a C-terminal domain that promote membrane association (Feiguelman et al., 2018). GEF clustering at membrane surfaces is another important layer of localization control, enabled by diverse types of interactions with integral membrane proteins, scaffolding proteins or via specific phospholipid-binding activity (Kozubowski et al., 2008; Meca et al., 2019; Shichrur and Yalovsky, 2006). For example, plant PRONE-domain ROPGEFs are clustered at the plasma membrane via physical interactions with receptor-like kinases that phosphorylate PRONE domain GEFs to relieve auto-inhibition (Duan et al., 2010; Kaothien et al., 2005; Zhang and McCormick, 2007). In the well-known metazoan Dbl homology (DH)-Pleckstrin homology (PH) domain GEFs, the lipid-binding activity of the PH domain is required to concentrate nucleotide exchange activity at the cell periphery (Chen et al., 1997; Karlovich et al., 1995; Zheng et al., 1996).

The more recently discovered Rac/ROP GEFs of the dedicator of cytokinesis (DOCK) family are evolutionarily conserved in the plant and animal kingdoms, and are defined by a tandem DHR1-targeting domain followed by DHR2, a catalytic domain of the DOCK family GEFs, in which nucleotide exchange activity resides (Cote and Vuori, 2002; Cote et al., 2005; Meller et al., 2005; Qiu et al., 2002). DOCK functions are often linked to cytoskeletal dynamics that mediate cell shape change and/or cell-cell interactions across a wide range of developmental contexts (Hasegawa et al., 1996; Liu et al., 2020; Nolan et al., 1998; Qiu et al., 2002; Ren et al., 2016; Wu and Horvitz, 1998). All plant genomes assembled to date encode SPIKE1 (SPK1) orthologs (Fig. S1A; Bascom et al., 2019; Qiu et al., 2002). One function of this master regulator is to physically interact with and cluster the WAVE/SCAR complex that activates the actin filament nucleator actin-related protein 2/3 (ARP2/3) (Basu et al., 2008; Kotchoni et al., 2009; Qiu et al., 2002; Yanagisawa et al., 2013). SPK1 functions at plasma membrane-anchored organelles of unknown identity, and at these signaling nodules, SPK1 integrates cortical actin polymerization with microtubule localization to pattern cellular-scale trafficking patterns and polarized growth (Yanagisawa et al., 2018, 2015; Zhang et al., 2010, 2013). Remarkably, despite the different cellular functions of cortical actin in metazoan and plant cells, animal cells may also use DOCK-SPK1 family GEFs to cluster and activate the WAVE/SCAR complex in neurons (Namekata et al., 2010).

All DOCKs are likely to be fully activated at specialized organelle surfaces; however, the membrane targeting mechanisms

[1]Departments of Botany and Plant Pathology, Purdue University, West Lafayette, IN 47907, USA. [2]Center for Plant Biology, Purdue University, West Lafayette, IN 47907, USA. [3]Department of Plant & Microbial Biology, North Carolina State University, Raleigh, NC 27695, USA. [4]Department of Biological Sciences, Purdue University, West Lafayette, IN 47907, USA.
*These authors contributed equally to this work
‡Deceased

§Author for correspondence (szymandb@purdue.edu)

E.L.M., 0000-0002-0363-5920; M.Y., 0000-0003-1824-2326; C.Z., 0000-0003-0985-7185; Y.L., 0000-0001-5260-0153; J.M.A., 0000-0001-7087-1571; D.B.S., 0000-0001-8255-424X

Handling Editor: Michael Way
Received 31 January 2022; Accepted 11 February 2022

Journal of Cell Science (2022) 135, jcs259825. doi:10.1242/jcs.259825

within the superfamily are poorly understood. The central DHR1 domain has been shown to directly bind phosphoinositol(3,4,5)triphosphate [PI(3,4,5)P3], and this clusters a small subpool of the protein at the plasma membrane (Cote et al., 2005). DHR1 contains a C2-like domain and conserved positively charged amino acids that are predicted to mediate specific interactions with PI(3,4,5)P3 (Premkumar et al., 2010). A subgroup of metazoan DOCKs [DOCK-A/B (HsDOCK1-5)] contain an N-terminal SH3 domain and a C-terminal proline-rich polybasic domain that bind to the regulatory protein engulfment and cell motility protein 1 (ELMO1) and the phospholipid phosphatidic acid, respectively (Gumienny et al., 2001; Nishikimi et al., 2009; Thompson et al., 2021). The dual lipid-binding activities of the DHR1 and polybasic domains may enable DOCK-A/B orthologs to integrate multiple signaling inputs in their localization control schemes (Nishikimi et al., 2009; Sanematsu et al., 2013). Most eukaryotic DOCK-C/D orthologs, including all in the plant kingdom, lack SH3 and C-terminal polybasic domains, and their localization control mechanisms are unknown (Fig. S1A; Jimenez-Sanchez, 2016; Thompson et al., 2021).

In leaf trichoblasts, SPK1 reversibly clusters at plasma membrane-anchored 'signaling nodules' to organize cellular-scale actin networks via the WAVE/SCAR and ARP2/3 complexes (Yanagisawa et al., 2018, 2015). In this study, we used combinations of transgene complementation, live-cell imaging and lipid-binding assays to discover a dual targeting mechanism that involves a domain termed DHR3-MOD1 (Qiu et al., 2002), which appears to have been conserved in a wide array of plant and animal species that diverged more than a billion years ago (BYA). We showed that the tandem DHR3 and DHR1 domains were necessary for the *in vivo* function and localization of SPK1. The isolated DHR3 fragment, which likely adopts a C2-domain-like conformation, clustered at organelle surfaces, and bound selectively to an array of negatively charged phospholipids. Our results indicate that coordinated activities of DHR3-C2 and DHR1-C2 are conserved features of the most ancient clade of DOCK family GEFs.

RESULTS

Orthologs in the DOCK-C family GEFs have been retained in both the plant and animal kingdoms (Fig. S1B). In the plant kingdom, SPK1 orthologs largely reflected speciation events (Fig. S1A). The orthologs from the monocot *Oryza nivara* and the simple non-vascular bryophyte *Physcomitrella patens* [the latter diverged from dicots about 450 million years ago (MYA) (Kumar et al., 2017)] shared 73% and 58% end-to-end identity with *Arabidopsis thaliana* SPK1, respectively. SPK1 is the most important GEF in moss, based on a reverse genetic analysis of ROP regulators (Bascom et al., 2019). Unicellular algae diverged from dicots ∼870 MYA, and *Ostreococcus tauri* and *Micromonas pusilla* orthologs shared only ∼20% identity with SPK1. Plants and animals diverged about 1.4 BYA. Metazoan DOCK6/7/8 orthologs are more similar to the plant proteins compared to the DOCK9/10/11 clade (Fig. S1B). *Arabidopsis* SPK1 was ∼22% identical to *Homo sapiens* DOCK7 following 1.4 billion years of divergence, perhaps reflecting a lower limit of sequence conservation needed to retain DOCK GEF functionalities.

Amino acid conservation among the orthologs was slightly higher in the dock homology region (DHR)1/C2 and DHR2 domains, which are diagnostic of the DOCK superfamily and recognizable as distinct domains (Fig. S1A). An additional patch of elevated sequence conservation N terminal to DHR1, termed DHR3-MOD1, has been noted in SPK1 orthologs (Qiu et al., 2002; Wang et al., 2018); however, existing domain search tools fail to identify a known sequence feature in this region of metazoan DOCK-C family members (Thompson et al., 2021). We used a diverse collection of DOCK-C orthologs to detect a DHR3-MOD1 region in SPK1 in which numerous residues were conserved across the plant and animal kingdoms (Fig. 1B). DHR3 maps near a domain with a C2-like fold in DOCK2 and DOCK5 that has no known function (Chang et al., 2020; Kukimoto-Niino et al., 2021), and may have a C2-like structure (see below).

In animal DOCKs, the DHR1 and its associated C2 domain mediate membrane interactions and promote protein clustering at the cell cortex (Cote et al., 2005; Premkumar et al., 2010). In order to investigate the significance of additional targeting domains in *Arabidopsis* SPK1, a series of protein deletions were tested for functional activity and localization. Transgenes using native genomic sequences to drive the expression of YFP-tagged SPK1 completely and efficiently rescue all *spk1* null phenotypes, and enable protein localization to known actin filament nucleation sites in living trichomes (Yanagisawa et al., 2018). Lines harboring the full-length YFP:SPK1 transgene accumulated a fusion protein of the expected size (Fig. 1A; Fig. S1D) and rescued the whole plant phenotype, and reduced the trichome branch phenotype of the *spk1* background (Fig. 1C). A recombineering approach was taken to generate specific domain deletions in the context of the full-length YFP:SPK1 protein (Zhou et al., 2011), as only the genomic clone in the context of ∼60 kB of native genomic sequence has been able to rescue the phenotype without causing gene silencing and loss-of-function phenotypes (Yanagisawa et al., 2018). It was technically challenging to generate a collection of ΔDHR1, ΔDHR3, ΔDHR1ΔDHR3 and ΔDHR2 truncation constructs because the large insert-transformation efficiency is low, but we focused initially on ΔDHR3. To test for residual activity of the ΔDHR3 deletion, it was transformed into the weak *spk1-666* allele that is of normal stature and fertile but has a trichome branch number reduction phenotype. Seven independent transformed lines that harbored the ΔDHR3 construct were confirmed for YFP trichome expression and rescue. The *spk1-666* plants displayed an increased number of two-branched trichomes compared to the wild type (Fig. S1C). All seven YFP-ΔDHR3SPK1-expressing lines had a phenotype that was indistinguishable from *spk1-666* (Fig. S1C). Given the increased level of amino acid sequence conservation in the DHR3 domain of SPK1 orthologs in the plant kingdom, this was an expected result.

We wanted to closely analyze the localization of ΔDHR3 and the other constructs in the absence of endogenous SPK1 protein. For this purpose, ΔDHR3 and the other constructs were either transformed or crossed into *spk1*/SPK1 heterozygous plants (because *spk1* homozygotes are completely sterile). For all of the deletion constructs, the transformed lines contained a single T-DNA insert based on 3:1 inheritance of the Basta resistance selectable marker. Whole-leaf protein extracts from individual *spk1* Basta-resistant plants were probed in western blots to determine whether fusion proteins of the expected size were detectable. Proteins of the correct size for each deletion construct were detected in whole-leaf extracts (Fig. S1D). Protein levels appeared to be reduced for the deletion constructs relative to the homozygous wild-type and full-length YFP:SPK1 lines; however, the *spk1* Basta-resistant plants were segregating for the transgenes and may contain either one or two copies. As a more reliable comparison of the levels of the SPK1 deletion proteins, live-cell imaging experiments in trichomes were conducted using nearly identical imaging settings (Fig. 1D-I).

Journal of Cell Science (2022) 135, jcs259825. doi:10.1242/jcs.259825

Among a population of early-stage trichomes, YFP signal of similar brightness was detected in all of the lines, suggesting that trichome-specific expression levels were similar among the constructs. None of the deletion constructs seemed to harbor any detectable functional gene activity because the *spk1* null syndrome of reduced stature, altered leaf shape (Fig. 1C) and reduced trichome branching segregated 3:1 in the lines segregating for the T-DNA constructs (χ^2 tests, N>85 in all cases, P>0.05). Truncation of the DHR2 domain eliminates ROP-binding and GEF-activity, and was expected to be non-functional (Basu et al., 2008). The lack of wild-type function for the DHR1 and DHR3 deletion constructs could affect SPK1 recruitment to membrane surfaces.

In wild-type trichomes, SPK1 is efficiently recruited to unstable cortical punctae that are concentrated at the cell apex during the cell tapering process (Yanagisawa et al., 2018). Most punctae are concentrated at the apex, but a co-occurrence of SPK1 punctae at subcortical locales was observed in three of 13 tapering trichomes (Fig. 1D). In young *spk1* trichomes ΔDHR3, 68% (N=57) of the cells had a punctate localization; the remainder had a hazy diffuse signal that reflected a cytosolic localization (Fig. 1E). Within a given cell, ΔDHR3 punctae were usually distributed between cortical and subcortical locales; however, approximately one-third of the cells with an organelle-associated pool had punctae that were exclusively subcortical. Many of the ΔDHR3$^+$ punctae organelles were highly motile (Movie 1). This reflects long distance actomyosin-dependent organelle transport, which is a basic characteristic of plant cells (Ryan and Nebenfuhr, 2018). Subcortical SPK1$^+$ organelles are inactive for WAVE/SCAR-ARP2/3 activation, and can be generated when an anchored organelle becomes detached and enters the long distance actomyosin-dependent trafficking system (Yanagisawa et al., 2018). These data indicate that ΔDHR3$^+$ punctae correspond to an inactive SPK1 pool.

ΔDHR1 had a more severe effect on localization. Although 81% (N=21 cells) had a completely diffuse localization pattern (Fig. 1F), the remainder contained sparse intracellular punctae that were distributed between cortical and subcortical sites. ΔDHR1 was tested for residual gene function by transforming it into the weak *spk1-666* background, and as expected the trichome phenotypes of ΔDHR1 *spk1-666* were indistinguishable from *spk1-666* alone (Fig. S1C). Compared with ΔDHR1, the ΔDHR1ΔDHR3 construct had a slightly higher percentage of cells, with a diffuse localization (90%, N=42; Fig. 1G). Taken together, these results indicate that DHR1 is the primary localization determinant, and DHR3 performs a secondary and perhaps sequential function to enable SPK1 to concentrate at cortical-anchored signaling nodules. The ΔDHR2 fusion protein retained its ability to be clustered at membrane surfaces in 91% of the cells (N=42), but surprisingly only 5/42 cells (usually very young *spk1* trichomes) retained the ability to cluster ΔDHR2 punctae at the cell apex (Fig. 1H). In most cases ΔDHR2 localized to punctae that were randomly distributed between cortical and subcortical locations (Fig. 1I). Interestingly, when ΔDHR2 was imaged in wild-type cells expressing at least one wild-type dose of *SPK1*, an apical concentration of punctae was not observed in 28 stage-4 trichomes with a blunt tip morphology, suggesting that the wild-type protein completely outcompeted ΔDHR2 for specialized membrane binding/organelle interaction sites at the apex.

These data suggest that both DHR3 and DHR1 contribute to the clustering of SPK1 to membrane surfaces and might bind to lipids. We next tested SPK1 for lipid-binding activity, as well as an N-terminal fragment (SPK1N) that contained the DHR3 domain and could be expressed in a soluble form. When the full-length SPK1 protein was expressed using a baculovirus expression system (Basu et al., 2008), it specifically bound to a subset of anionic lipids, including phosphatidylinositol (PI), its monophosphorylated forms (PI3P, PI4P and PI5P) and phosphatidylserine (PS) (Fig. 2A). The SPK1N fragment had a very similar pattern as the full-length protein, except that PI was not bound (Fig. 2B). The binding of both SPK1 and SPK1N was selective for PS and the type of fatty acid chain, as both proteins bound specifically to dipalmitoyl-PS (DPPS), but not PS prepared from soybean, which contains ∼70% 18:2 linoleic acid (Fig. 2C). No such fatty acid chain selectivity was observed with the known PS-binding protein ANNEXINV (Fig. S2C). The lipid-binding activity of SPK1 and SPK1N were analyzed further in a series of liposome co-sedimentation assays. (Fig. 2D). SPK1N was efficiently sedimented by liposomes containing DPPS but no binding was detected with the carrier lipid dipalmitoyl-phosphatidylcholine (DPPC) (Fig. 2E). At a range of lipid concentrations, SPK1N binding was highly selective for DPPS, because no binding was detected independent of the carrier lipid and was not detected with either soybean PS or soybean PI as the test lipid. Also, unlike the binding of ANNEXINV, SPK1N binding to PS was Ca^{2+}-independent (Fig. S2B). This was expected as many of the C2 domain-containing proteins that are members of the ancient DOCK clade have not retained Ca^{2+}-binding activity (Zhang and Aravind, 2010).

Phospholipids are required for SPK1 apical clustering because wortmannin, an effective phosphoinositide 3-kinase (PI3K) inhibitor in plants (Vermeer et al., 2006), efficiently decreased the degree of SPK1 clustering in the branch apex compared to DMSO controls (Fig. 2F,G). When seedlings were incubated in buffer controls with 0.5% DMSO, 15/15 stage 4 trichomes had tip signal that was indistinguishable from the wild type. When treated with wortmannin, only one of 25 trichomes displayed tip signal, and that cell only had one branch with dim signal. The effect was reversible upon drug washout (Fig. 2H-J). These results suggest that PI3K is required to locally cluster SPK1 at cortical punctae; however, the effect could be mediated either by reduced levels of phosphatidylinositol 4,5-bisphosphate (PIP) and/or PS (Chung et al., 2015; Moser von Filseck et al., 2015). The identity of the particular lipids and organelle systems involved in compartmentalized SPK1 signaling remains to be determined.

To characterize the ability of SPK1 N-terminal regions to mediate organelle association *in vivo*, protein fragments of various lengths were tagged with GFP and expressed in *Arabidopsis*. SPKN1 corresponds to the first half of SPK1, and contained both DHR3 and DHR1, whereas SPKN2, SPKN3 and SPKN4 contained the DHR3 region and additional flanking sequences (Fig. 3A). Overexpression caused SPK1 gene silencing and loss-of-function phenotypes, so all constructs were expressed in the *rdr6* background to generate lines with patchy expression in young seedlings. GFP controls had a diffuse and mottled appearance that reflected the uneven distribution of cytosol in vacuolated epidermal cells in the cotyledon and hypocotyl (Fig. 3C,D). All of the GFP-SPK1-N-terminal fragments had a similar localization, with the fusion proteins partitioned between cytosolic and organelle-associated pools (Fig. 3C,D). The punctate localization is due to an organelle association and not non-specific protein aggregation, because GFP:SPK1N2 colocalized with CFP:PTS1 (Nelson et al., 2007), a known peroxisome marker (Fig. 3E). Therefore, DHR3 is sufficient for organelle association *in vivo*; however, this localization pattern was not necessarily related to that of endogenous SPK1 because the SPK1N2 and SPK1N3 fragments had only a diffuse localization in young trichomes. It was possible to partially purify small amounts of recombinant SPK1N3 (Fig. S2A). In the lipid overlay assay, the SPK1N3 fragment displayed a lipid-binding selectivity for monophosphorylated

Journal of Cell Science (2022) 135, jcs259825. doi:10.1242/jcs.259825

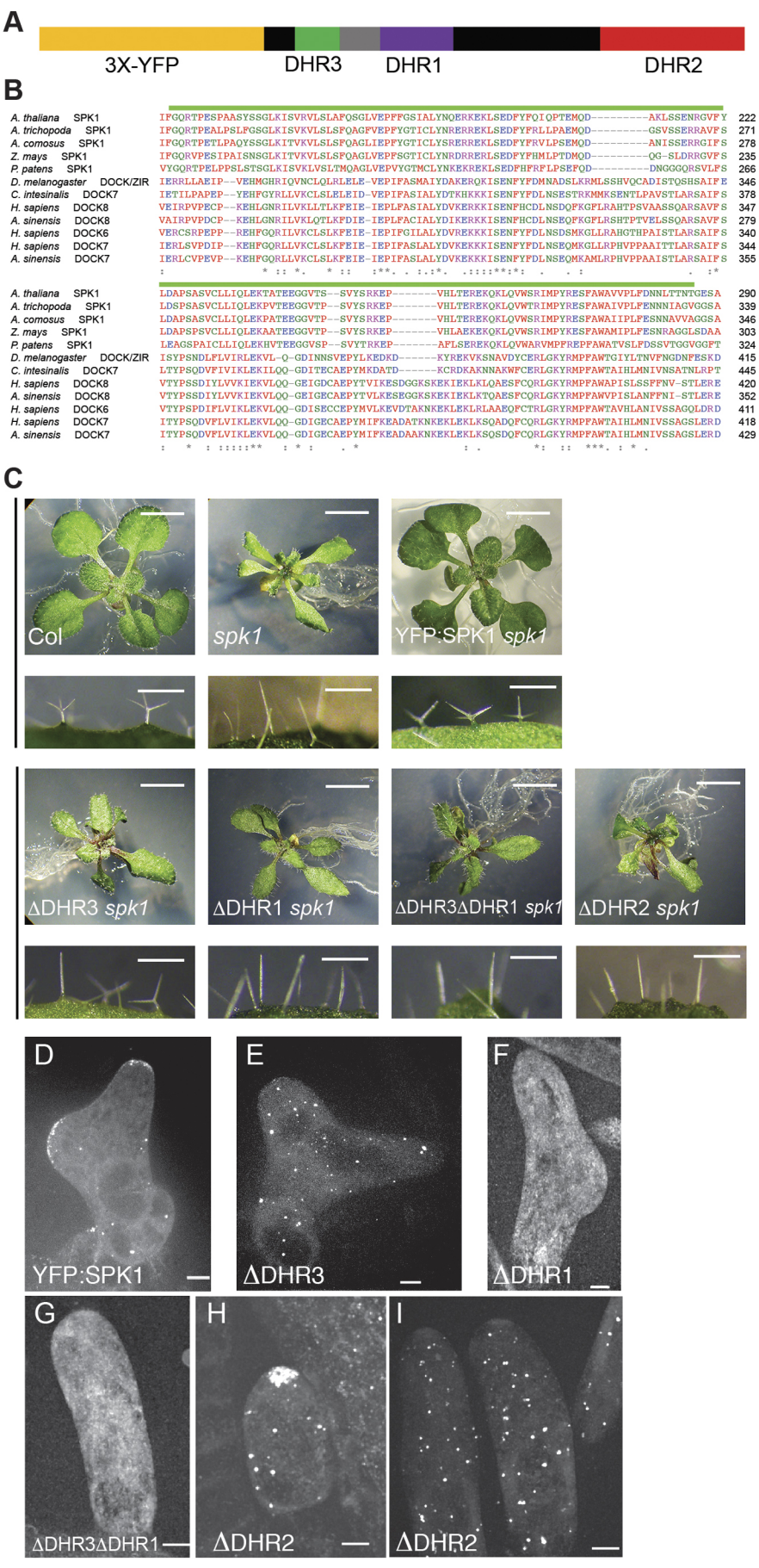

Fig. 1. Functional analysis of SPK1 domains. (A) Domain organization of tagged SPK1 and location of the domains that were mutated in transformation and rescue experiments. The N terminus includes three copies of YFP. DHR3 includes amino acids 136-286; DHR1 includes amino acids 450-728; and DHR2 includes amino acids 1300-1830. (B) Multiple sequence alignment of the DHR3 domain in selected plant DOCK GEFs and animal DOCK GEFs within the DOCK-C clade (Thompson et al., 2021). Sequences of SPK1 and DOCK orthologs were aligned using Clustal Omega at the EMBL-EBI website (www.ebi.ac.uk/Tools/msa/). Estimated conservation of amino acids was reported using '*' (a single fully conserved residue), ':' (scoring >0.5 in the Gonnet PAM 250 matrix) and '.' (≤0.5 and >0) symbols. (C) Phenotypic rescue analyses of SPK1 deletions. Paired images of whole plants and example trichome images. Upper panels: Col wild-type, *spk1* mutant and functional YFP-tagged SPK1 expressed in the *spk1* background. Lower panels: DHR3 deletion mutant expressed in *spk1*, DHR1 deletion mutant expressed in *spk1*, double deletion mutant of DHR3 and DHR1 in *spk1*, and DHR2 truncation mutant in *spk1*.
(D-I) Localization of SPK1 and deletion constructs in early stage trichomes. All constructs were expressed in *spk1* null plants. (D) YFP-SPK1 localization to cortical punctae that are concentrated at the apices of developing branches. (E) Localization of DHR3-deletion proteins to subcortical punctae distributed throughout the cytoplasm. (F) Diffuse localization of DHR1-deletion mutant proteins. (G) Diffuse localization of DHR3- and DHR1-double deletion mutant proteins. (H) Example image of DHR2 truncation protein with apical clustering and subcortical punctae. (I) Example image of DHR2 truncation protein localizing to subcortical punctae. Scale bars: whole seedling images, 5 mm, trichome images, 0.5 µm (C); 5 µm (D-I).

Journal of Cell Science (2022) 135, jcs259825. doi:10.1242/jcs.259825

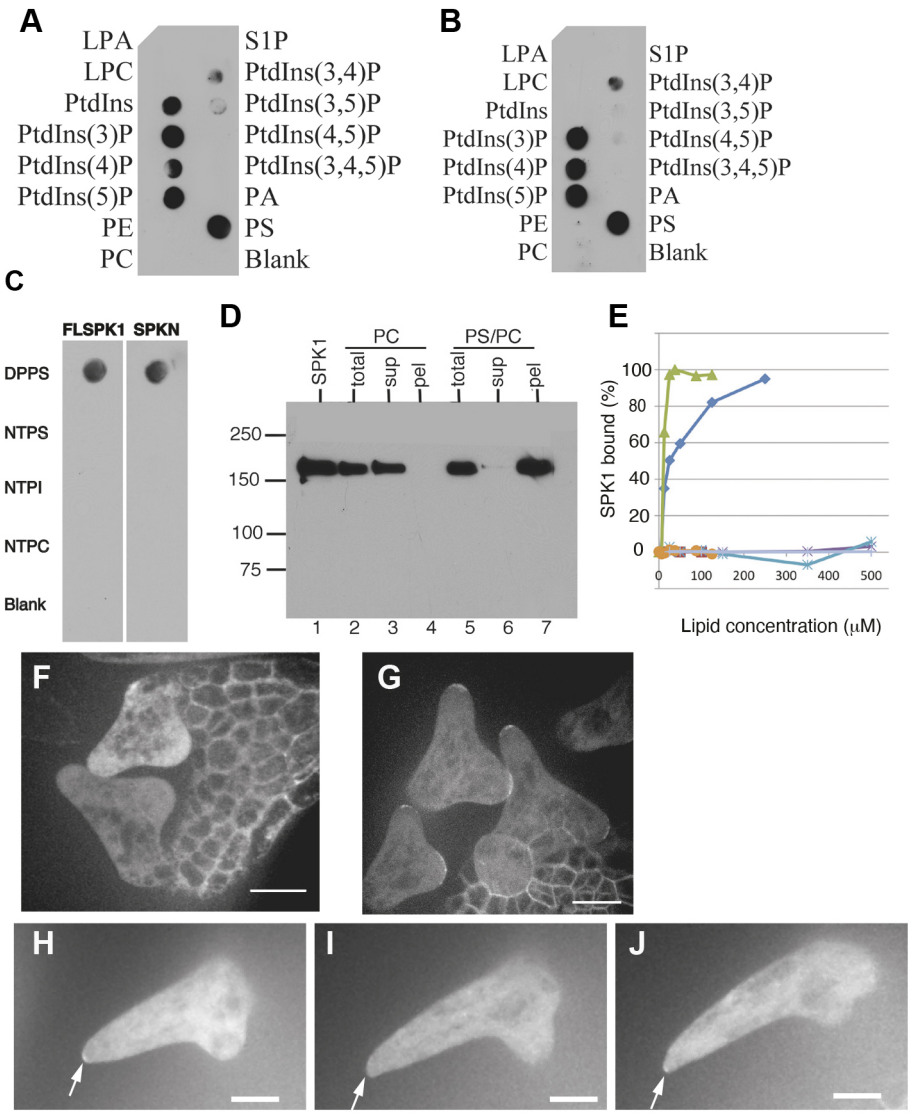

Fig. 2. SPK1 binds to different phospholipids via its N-terminal region. (A) Lipid-protein overlay assay of SF9 insect-expressed full-length SPK1 protein with PIP strip. (B) Lipid-protein overlay assay of partially purified his-tagged SPKN (amino acids 1 to 312) protein with PIP strip. (C) SPK1 and SPK1N binding are sensitive to the degree of lipid saturation. Lipid-protein overlay assay of SF9 insect-expressed full-length SPK1 (left) and SPKN protein (right) with DPPS; natural (soy) PS (NTPS); natural (soy) PI (NTPI); natural (soy) PC (NTPC); and blank (no lipid control). (D) Full-length SPK1 protein co-sediments with liposomes of 50% DPPS/50% DPPC. Full-length SPK1 protein (25 nM) was incubated with liposomes containing 90 µM PS/90 µM PC or 180 µM PC. The separated pellet and supernatant fractions were loaded as equal proportions. Lane 1 was 22 ng full-length SPK1, which was used as the loading control. Lane 2 to lane 4 are the total, supernatant (sup) and pellet (pel) fractions of SPK1 co-sedimented with PC liposomes. Lane 5 to lane 7 are the total, supernatant and pellet fraction of SPK1 co-sedimented with PS/PC liposomes. The protein standards in kDa are shown. (E) The SPK1N fragment binds selectively to PS with saturated fatty acids in liposome binding assays. All binding reactions conducted with the SPK1N fragment. Green, DPPS/NTPC; dark blue, DPPS/DPPC; orange, NTPI/NTPC; cyan, DPPC/NTPC; purple, NTPS/NTPC; light blue, NTPC; and red (partially obscurred along the *x*-axis), DPPC. (F) Wortmannin reduces SPK1 clustering at the cell apex. Stage 4 trichomes treated with 50 µM wortmannin for 3 h consistently displayed reduced tip signal compared to controls. (G) Control imaging results when YFP:SPK1 seedlings are mounted in 0.5% DMSO. (H) Wortmannin inhibition of tip localization is reversible. Longitudinal axial midplanes of a tapered branch with tip localization. (I) The same cell after 50-µM wortmannin treatment for 1 h 40 min. (J) Tip signal recovery in the same cell after the removal of wortmannin and recovery in DMSO for an additional 1 h 45 min (F,G). Arrows in H-J indicate the trichome branch apex. Scale bars: 20 µm (F,G); 10 µm (H-J). DPPC, dipalmitoyl phosphatidylcholine; DPPS, dipalmitoyl phosphatidylserine; LPA, lysophosphatidic acid; LPC, lysophosphocholine; NTPS, natural PS from soybean; NTPI, natural PI from soybean; PA, phosphatidic acid; PC, phosphatidylcholine; PE, phosphatidylethanolamine; PtdIns, phosphatidylinositol; PtdIns(3)P, PtdIns 3-phosphate; PtdIns(4)P, PtdIns 4-phosphate; PtdIns(5)P, PtdIns 5-phosphate; PtdIns(3,4)P, phosphatidylinositol 3,4-bisphosphate; PtdIns(3,5)P, phosphatidylinositol 3,5-bisphosphate; PtdIns(4,5)P, phosphatidylinositol 4,5-bisphosphate; PtdIns(3,4,5)P, phosphatidylinositol 3,4,5-trisphosphate; PS, phosphatidylserine; S1P, sphingosine-1-phosphate.

phosphoinositides and PS (Fig. 3B). Therefore binding activity resides within DHR3, and it had lipid-binding activity that was indistinguishable from the larger SPK1N fragment (Fig. 2B).

We took advantage of new protein structure prediction resources to visualize atomic structures for SPK1 and its DHR3 domain. The complete SPK1 structure predicted from AlphaFold (Fig. 4; Fig. S3A; Jumper et al., 2021) and that of SPK1 amino acids 1 to 1117 predicted using RoseTTAFold (Fig. S3B; Baek et al., 2021) were qualitatively very similar to each other and to the solved structures for human DOCK proteins (Chang et al., 2020; Kukimoto-Niino et al., 2021). The predicted SPK1 protein adopted an extended conformation, with the C-terminal catalytic DHR2 domain

Journal of Cell Science (2022) 135, jcs259825. doi:10.1242/jcs.259825

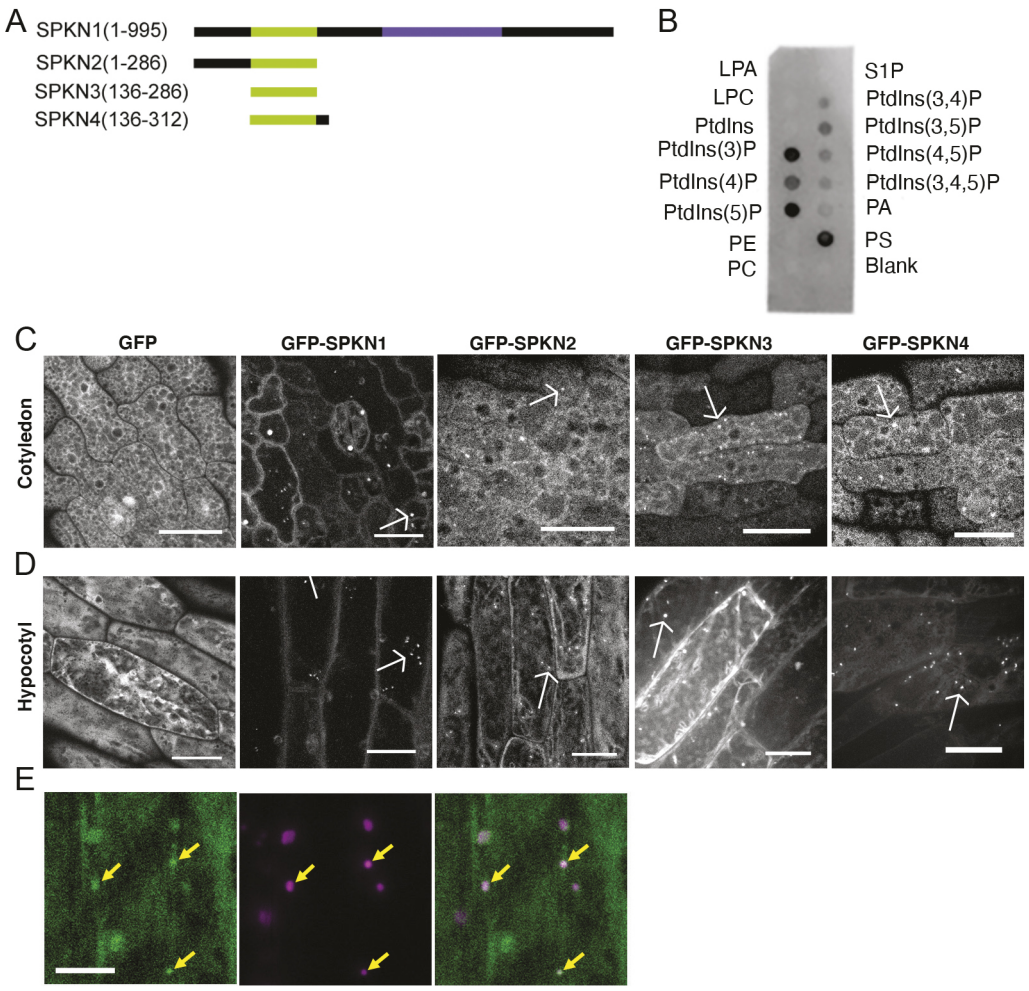

Fig. 3. The DHR3 domain has lipid-binding activity and is sufficient for organelle association *in vivo*. (A) Summary of N-terminal SPK1 fragments that were tested for *in vivo* associations with organelles. Amino acid residues for each fragment are listed and the DHR3/C2 region is colored green. (B) Lipid blot overlay showing binding specificity of the SPK1 N3 protein fragment. (C) Localization of free GFP (far left) and the indicated SPK1 N-terminal fragments in rdr6 plants 2 days after germination (DAG) in cotyledon pavement cells. The identity of the SPK1 fragment that was fused at its N terminus with GFP is indicated above each image. (D) Localization of free GFP (far left) and the indicated SPK1 N-terminal fragments in 3-DAG hypocotyl epidermal cells. SPK1 fragments indicated as in panel C. Arrows label instances of punctate localization. (E) Two-color live-cell imaging of GFP:SPK1N2 (left), the peroxisomal marker CFP:PTS1 (middle) and the overlayed images. Arrows indicate example peroxisomes displaying colocalization. Scale bars: 10 µm. LPA, lysophosphatidic acid; LPC, lysophosphocholine; PA, phosphatidic acid; PC, phosphatidylcholine; PE, phosphatidylethanolamine; PtdIns, phosphatidylinositol; PtdIns(3)P, PtdIns 3-phosphate; PtdIns(4)P, PtdIns 4-phosphate; PtdIns(5)P, PtdIns 5-phosphate; PtdIns(3,4)P, phosphatidylinositol 3,4-bisphosphate; PtdIns(3,5)P, phosphatidylinositol 3,5-bisphosphate; PtdIns(4,5)P, phosphatidylinositol 4,5-bisphosphate; PtdIns(3,4,5)P, phosphatidylinositol 3,4,5-trisphosphate; PS, phosphatidylserine; S1P, sphingosine-1-phosphate.

connected to DHR1 (containing a C2-like domain) via an extended structure that resembled armadillo repeats (ARM) that are similar to solved structures for human DOCKs (Chang et al., 2020; Kukimoto-Niino et al., 2021; Premkumar et al., 2010; Yang et al., 2009). The predicted SPK1 molecule has an overall elongated shape with a slightly cupped C terminus and a maximum length of 20 nm (Fig. 4B,C). The AlphaFold atomic structure of SPK1 was used in a series of Dali searches for similarities to solved protein structures. Human DOCK10 was the highest scoring hit, with highly significant similarities in the ARM and DHR2 domains (PDB code 6TKY, Z score 35.1, RMSD of 2.7 Å over 403 Cα atoms; David Barford, unpublished). The DHR1 region of DOCK8 was the second-best hit (PDB code 7CLX, Z score, 16.5; RMSD of 3.3 Å over 153 Cα atoms; Sakurai et al., 2021).

The SPK1 DHR3 also had a C2-like structure that was tightly appressed to DHR1-C2 (Fig. 4D; Fig. S3A,B). C2 folds resemble a β-sandwich comprising two β-sheets with four strands each (Hurley and Misra, 2000). Two of the predicted β-strands and intervening alpha helices were outside DHR3, and this extended region was appended to DHR3 and defined as DHR3-C2 (Fig. 4A,D; Fig. S3A-C); however, these additional amino acids were not essential for lipid binding or organelle localization (Fig. 3). The DHR3-C2 domain was used in a Dali search and again identified DOCK8 DHR1-C2 as the closest match (PDB code 7CLX, Z score of 12.1, RMSD of 3.5 Å over 140/180 Cα atoms/aligned residues). C2 domains often bind to anionic lipids through a patch of electrostatic interactions. The predicted SPK1 DHR3-C2 domain had a large electropositive patch that was in the same plane as another electropositive patch in the DHR1-C2 domain (Fig. 4E-G). Interestingly, numerous highly conserved basic amino acids in the DHR3/C2 domain were clustered within the exposed electropositive region, potentially forming sites of specific phospholipid binding (Fig. 4H). Similarly positioned C2 domains are present in DOCK-A/B orthologs (Chang et al., 2020; Kukimoto-Niino et al., 2021). We found that ∼74% of the residues that were conserved in the DHR3-C2 domain of plant SPK1 and metazoan DOCK-C orthologs (Fig. 1B)

Journal of Cell Science (2022) 135, jcs259825. doi:10.1242/jcs.259825

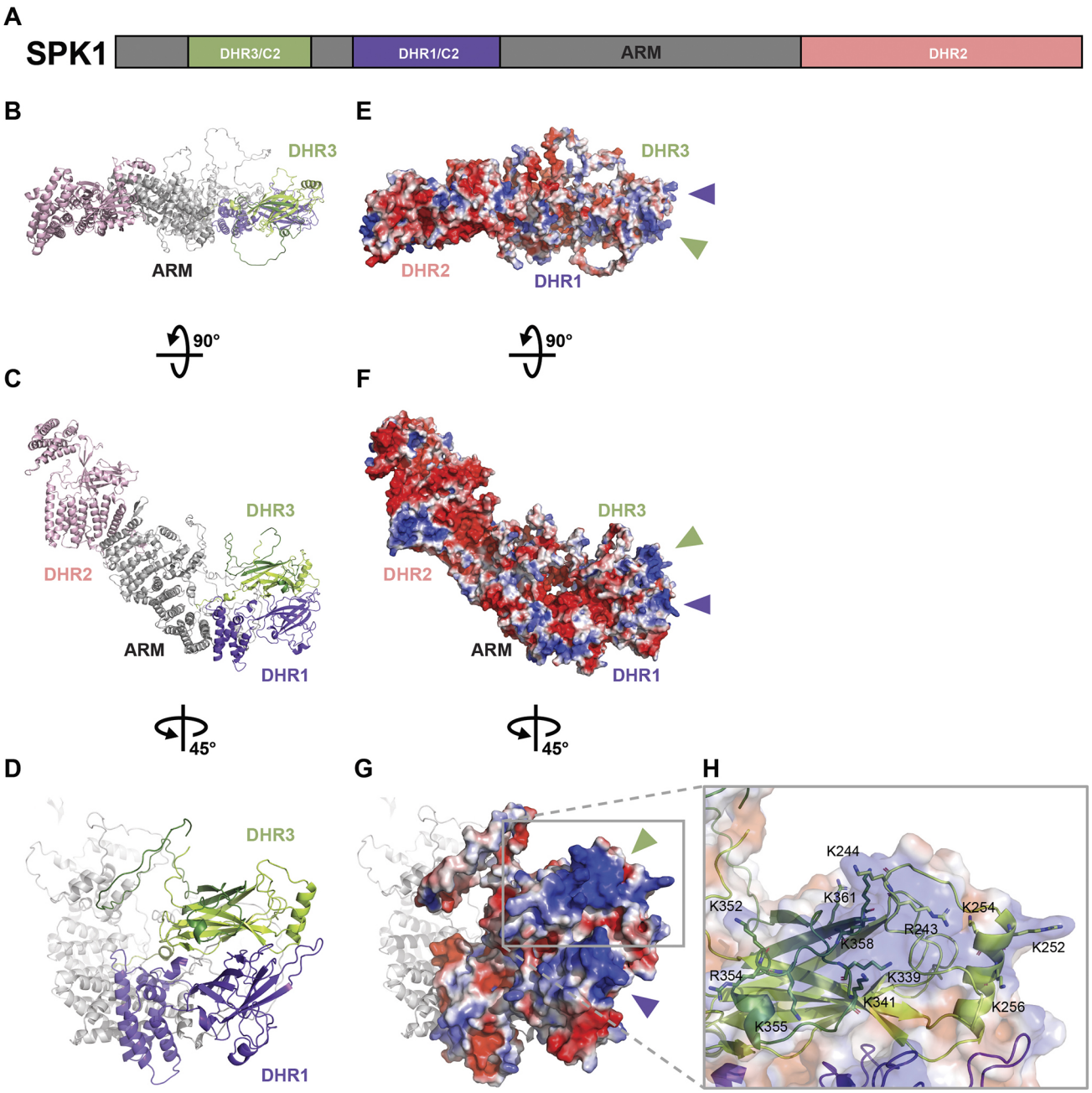

Fig. 4. An atomic structure model of SPK1 and its DHR3/C2 domain. The predicted SPK1 protein structure was downloaded from the AlphaFold Protein Structure Database built with AlphaFold v2.0 (last updated on July 1, 2021). The model confidence level was marked as confident (90>pLDDT>70). (A) Schematic domain structure of SPK1 indicating the presence of two predicted C2 domains. The known ARM, DHR1 and DHR2 of experimentally determined DOCK structures are shown. (B,C) Two views of the predicted SPK1 fold are visualized in the ribbon diagram using the color scheme in A. (D) Magnified views of the adjacent DHR3 and DHR1 domains. (E-G) The surface electrostatic potentials of SPK1 in the same views shown in B-D. The positively charged patches are labeled with triangles consistent with domain colors (+ is blue, – is red). (H) Zoomed-in view of the boxed region in G showing the positions of conserved residues that were found in multiple sequence alignments in Fig. 1B.

were also present in DOCK-D orthologs (Fig. S3C). These data indicate that tandem DHR3-C2 and DHR1-C2 domains are a conserved feature of the DOCK superfamily.

DISCUSSION

DOCK GEFs have retained critical catalytic and localization control functions that enable effective signaling at the plasma membrane interface (Liu et al., 2020; Qiu et al., 2002; Ren et al., 2016; Uhrig et al., 2007; Wang et al., 2018; Yanagisawa et al., 2018). The DOCK superfamily radiated following a series of ancient gene duplication and neofunctionalization events to generate GEFs with a diverse array of domain organizations (Jimenez-Sanchez, 2016; Thompson et al., 2021). The SPK1-DOCK-C clade appears to be the most ancient and has been maintained in both plant and animal kingdoms (Fig. S1B). SPK1-DOCK-C GEFs display similar domain organizations and broad reactivities toward ROP/Rac-related GTPases (Basu et al., 2008; Miyamoto et al., 2007; Yamauchi et al., 2008); however, their localization control mechanisms and those of the DOCK superfamily in general are poorly understood. Here, we show that the DHR3-C2 domain is an

Journal of Cell Science (2022) 135, jcs259825. doi:10.1242/jcs.259825

evolutionarily conserved and essential localization determinant that operates in concert with the adjacent DHR1-C2 domain.

Numerous charged and hydrophobic residues in DHR3 are highly conserved across kingdoms (Fig. 1B; Fig. S3). The DHR3-containing region is predicted to adopt a C2-like beta sandwich fold (Fig. 4D), which defines the C2 domain (Hurley and Misra, 2000). Because C2 domains share very low levels of amino acid identity, many (such as those within the DHR3 region) escape identification (Zhang and Aravind, 2010). A DHR3-C2 domain upstream from DHR1 may be a universal feature of the DOCK superfamily. Recent cryo-electron microscope structures of the distantly related DOCKA orthologs DOCK2 and DOCK5 revealed a DHR3-C2 domain of no known function (Chang et al., 2020; Kukimoto-Niino et al., 2021). Based on its predicted lack of Ca^{2+}-binding activity and poor surface accessibility, DHR3-C2 has been proposed to mediate protein-protein interactions rather than protein-lipid interactions (Kukimoto-Niino et al., 2021). Animal DOCK-C/D orthologs share amino acid identity with plant DOCKs in the DHR3-C2 domains and likely adopt similar folds (Fig. 4D; Fig. S3C). Therefore, DHR3-C2 is a conserved feature of the superfamily, and our work establishes its critical role both for wild-type gene function (Fig. 1C), normal clustering at cortical active sites (Fig. 1E) and lipid/membrane interactions (Fig. 3).

The cortical sites correspond to active signaling nodules in which SPK1 drives W/SRC- and ARP2/3-dependent actin polymerization in the apical dome (Yanagisawa et al., 2018, 2015). These transient plasma-membrane anchored punctae may correspond to a specialized type of endoplasmic reticulum (ER)-plasma membrane contact site (Zhang et al., 2010). Deletion of DH3 redistributes SPK1 to an inactive subcortical pool of motile organelles, and DHR1 is necessary for this subcortical localization (Fig. 1E-G; Movie 1). Therefore, DHR1 appears to play a more prominent role in the basic recruitment of SPK1 to an organelle surface, which precedes DHR3-C2 lipid binding to enable normal membrane clustering and full activation. Certainly additional biochemical analyses of DHR1 lipid-binding specificity are needed, but to date we have been unable to generate soluble DHR1 protein fragments. However, if the PI binding activity of the full-length protein (Fig. 2A) reflects the primary DHR1 lipid-binding activity, localized PI may be the gateway of entry of cytosolic SPK1 into the endomembrane system.

DHR3 is sufficient for SPK1 organelle association (Fig. 3C,D); however, its role in membrane recruitment is likely to be complex. Effective recruitment to apical signaling nodules appears to require both the selective lipid-binding activities of DHR3, as well as some form of GEF-dependent positive feedback because SPK1ΔDHR2 failed to concentrate properly at the cell apex (Fig. 1H,I). The *in vitro* DHR3 lipid binding was selective for the major monophosphorylated phosphoinositides and PS (Figs 2, 3; Fig. S2). Binding activity of DHR3, but not the known PS-binder AnnexinV, was strongly sensitive to fatty acid chain saturation, perhaps reflecting partial membrane penetration and lipid sensing of the DHR3 fragment (Fig. 2C,E; Fig. S2C). Similar selectivities may be general features of DOCKs that retain highly conserved amino acids in the DHR3 region (Fig. 1B, Fig. 4H; Fig. S3). The involvement of PI3P-dependent lipids in SPK1 apical clustering is clear, based on the clear and reversible effect of wortmannin on SPK1 apical clustering (Fig. 2F-J). However, the details of which combinations of lipid species and organelle systems dictate the cycling behaviors of SPK1 (Yanagisawa et al., 2018) remain to be determined. The PS binding of DHR3 is of particular interest because PS concentrates in the inner leaflet of the plasma membrane and has been implicated in ROP-based hormone signaling (Platre et al., 2019).

In most cell types, DOCK GEFs associate with multiple cellular compartments, and the locations of active and inactive pools, and the membrane environments that control their cycling, are poorly understood. In cultured mammalian cells, multiple lipid signals are involved and the DHR1 and C-terminal PD domains mediate PIP3- and PA-dependent recruitment to the cell periphery, respectively (Nishikimi et al., 2009). Here, we discovered additional layers of control that involve DH3-C2. C2 is an ancient membrane-binding domain, and eukaryotic proteomes encode seven distinct clades (Zhang and Aravind, 2010). DHR1-C2 defines one of them. In signaling systems, C2 domains are frequently deployed in tandem (Corbalan-Garcia and Gomez-Fernandez, 2014; Meca et al., 2019), and our results indicate that the DHR3-C2 and DHR1-C2 domains evolved in tandem to generate sequential lipid-sensing activities that enable highly regulated membrane clustering. SPK1 colocalizes with ER exit site markers (Zhang et al., 2010), and active SPK1 dynamically clusters at plasma membrane-anchored signaling nodules (Yanagisawa et al., 2018). Given that PS is involved in ROP signaling and accumulates in the inner leaflet of the plasma membrane, and that DOCK proteins and SPK1 likely have the capacity to form antiparallel homodimers (Uhrig et al., 2007; Kukimoto-Niino et al., 2021), we speculate that the PS- and PIP-binding activities allow SPK1 to bridge two organelle systems. The failure of ΔDHR2 to cluster in cortical signaling nodules could reflect either the inability of the truncated protein to dimerize or a role for GEF activity and positive feedback in SPK1 clustering at these specialized sites. Future work will focus on determining how tandem C2 domains enable SPK1 complexes to sense compositional and biophysical membrane properties of organelle systems that modulate ROP signaling and ARP2/3 activation.

MATERIALS AND METHODS

Plant strains and growth conditions

Arabidopsis thaliana ecotype Columbia (Col) was used as the wild type in this study, and the reference spk1 allele was the previously published *spk1-1* null allele (Qiu et al., 2002). The weak allele *spk1-666* is a point mutant in the DHR2 domain in the Col-0 background. The *pss-1* allele is in the Col-0 background and corresponds to SALK_128223 (Arabidopsis Biological Resource Center, Columbus, OH). rdr6-11 *Arabidopsis* seeds were also obtained from the Arabidopsis Biological Resource Center (CS24285). For phenotyping, plants were grown on half-strength Murashige and Skoog medium containing 1% sucrose and 0.8% agar under continuous light (110 µmol m^{-2} s^{-1}) at 22°C. Low magnification images of whole-plant and trichome phenotypes were captured using a Leica MZ12.5 stereomicroscope (Leica Microsystems, Heerbrugg, Switzerland) with a Nikon Coolpix 4500 4× zoom digital camera (Tokyo, Japan).

Lipid protein overlay assays

The PIP strip membranes (Echelon Biosciences, Salt Lake City, UT, USA, P-6001) were blocked for 1 h at room temperature with 3% bovine serum albumin (BSA):TTBS {fatty-acid free BSA [Sigma-Aldrich, St Louis, MO, USA, A3803] in TTBS [50 mM Tris-HCl (pH 7.5), 150 mM NaCl and 0.1% Tween-20]}. Then, purified SPKN (1 mg), SPKN3 (1 mg) or crude insect cell extracts expressing full-length SPK1 (Basu et al., 2008) were incubated with the PIP strip in 10 ml 3% BSA:TTBS with a 1:100 dilution of protease inhibitor cocktail (1.6 mg/ml benzamidine HCL, 0.12 mg/ml phenanthroline, 1 mg/ml aprotinin, 1 mg/ml leupeptin and 1 mg/ml pepstatin A, Sigma-Aldrich) and 1 mM PMSF (Sigma-Aldrich, 78830) at 4°C overnight with gentle shaking. The next day the PIP strip was washed with TTBS three times for 10 min each time period. SPK1 proteins were detected with a 1:1000 dilution of a rabbit polyclonal SPKN antibody (Basu et al., 2008) that was incubated with the PIP strip in 3% BSA:TTBS at room

temperature for 1 h with shaking. The PIP strip was washed again three times for 10 min each time with TTBS. A horseradish peroxidase (HRP)-conjugated goat anti-rabbit IgG secondary antibody (Invitrogen, Carlsbad, CA, USA, 31460) was then added for 1 h with shaking at room temperature at a 1:50,000 dilution in 3% BSA:TTBS. Finally, the PIP strip was washed with TTBS three times for 10 min each time, and then with TBS for 5 min. The blots were then developed with Super Signal West Pico Plus chemiluminescent substrate (Thermo Fisher Scientific, Waltham, MA, USA, 34577) on X-ray film. To test for the selectivity of SPK1 to acyl chains on the phospholipids, 2 µg each of dipalmitoyl PS, soybean PS, soybean PI or dipalmitoyl PC were manually spotted onto nitrocellulose membrane and detected as described above. Chloroform was spotted as the blank control. Recombinant HIS-tagged ANXV was detected using an HIS6X mouse IgG antibody (Covance Research Products/BioLegend, San Diego, CA, USA, MMS-156P). PIP strip overlays with ANXV were conducted with and without 1.2 mM $CaCl_2$. All lipids with the 'natural' designation were isolated from soybean and contained 68% 18:2 linoleate; all other lipids primarily contained 16:0 palmitic acid.

Liposome co-sedimentation assays

For liposome production, calculated amounts of chloroform-dissolved lipids were mixed in a 50-ml round-bottom flask and then dried under flowing nitrogen gas with rotation to form a uniform lipid film. The lipid film was kept under vacuum for 2 h and then rehydrated in extrusion buffer [250 mM raffinose, 25 mM Tris-HCl (pH 7.5) and 1 mM dithiothreitol (DTT)]. The rehydrated lipid film was passed through a 100-nm pore size polycarbonate membrane 20 times. Three volumes of binding buffer (50 mM Tris-HCl, PH 7.5, 150 mM NaCl, 1 mM DTT) were added to the liposomes in extrusion buffer, and the solution was then centrifuged at 130,000 ***g*** for 30 min. The pelleted liposomes were resuspended in binding buffer to a final concentration of 1 mM. The resulting liposome stocks were diluted with binding buffer to the desired concentrations, with the test lipid making up 10% of the total lipid amount. The liposomes were then equilibrated with 50 nM SPK1N or 150 nM ANXV at 23°C (room temperature) for 30 min in 100-µl reactions. For ANXV, 1.2 mM $CaCl_2$ was included in the binding reaction. The liposomes were recovered by centrifugation at 130,000 ***g*** for 30 min at 4°C. The supernatant fraction from the ultracentrifugation was saved to detect unbound proteins that were quantified by densitometry of western blots of the bound (in the resuspended liposome fraction) and unbound (in the supernatant) fractions.

YFP:SPK1 recombineering and domain deletions

Four deletion mutants (*spk1Δdhr1*, *spk1Δdhr3*, *spk1Δdhr3Δdhr1* and *spk1Δdhr2*) were generated in the previously described *YFP-SPK1* construct (Yanagisawa et al., 2018) by recombineering (Zhou et al., 2011). Briefly, the positive-negative selectable recombineering cassette RPSL-Amp was amplified using the primers Spike1RPSL1F and Spike1RPSL123R to generate the amplicon RPSL-Amp-DDHR3, primers Spike-DHR1-RPSLF and Spike-DHR1-RPSLF to generate the amplicon RPSL-Amp-DDHR1, and primers Spike1RPSL4F and Spike1RPSL4R to generate the amplicon RPSL-Amp-c-terminus. The RPSL-Amp-DDHR3 insertion was then replaced by recombineering with either the commercially synthesized gBlockDDH3 to generate the *spk1-n-ddhr3* mutant or with the synthetic gBlockDDHR1 to generate the *spk1-m-ddhr1* mutant. The RPSL-Amp-c-terminus was replaced by the synthetic fragment gBlock-c-terminus to generate *spk1-c-terminus* mutant. Finally, the amplicon RPSL-Amp-DDHR1 was inserted in the *spk1-n-ddhr3* mutant construct and then replaced by the synthetic gBlock-DDHR1 sequence to generate *spk1-n-ddhr3-m-ddhr1*. All the primers and gBlocks were synthesized by Integrated DNA Technologies. The deletions were confirmed by sequencing using the primers SpikeTest123F and SpikeTest123F (*spk1-n-ddhr3*), Spike-DHR1-TestF and Spike-DHR1-TestR (*spk1-m-ddhr1*), SpikeTest123F and Spike-DHR1-TestR (*spk1-n-ddhr3-m-ddhr1*), and Spike-c-terminus-TestF and Spike-c-terminus-TestR (*spk1-c-terminus*). The primer sequences were as follows: gBlockDDHR3, 5′-CAGCATTTTGGGCAACCTCC-TTTACCTGCTTATGAACCAGCTTTTGACTGGGAAAATGAAAGA-GCTATGATTTTTACTGGTGAATCTGCTTCCCCTAGCAGTCCTCT-TGCTCCTAGTATGACTGCGTCAAGTTCCCATGATGGTGTTTAT-3′; gBlockDDHR1, 5′-GTGTCTAGTCCTTCATATAATTTGCTCGCAAAT-TGATATGTTTATCGTCTTTGGTTCCAGGCTTTTGATTTTTGCGAA-ACCCTTCAGGTTTTTCAACTGAAATCTTCTAGTTCCTTAGCATAA-AATTTTGTTAAAAGCAATCTTGTCTCT-3′; gBlock-c-terminus, 5′-C-GAGTGTTTGATCGTTTCTTATTTGACACACCATTTACGAAAAATG-GTAAAACCCAAGGTGGATTAGAAGATCAATAGTGTATCTTTGTC-AGTTTTTGTTACGAGTTTTGTGCTTTTTTCTTCCACCATTTGGCT-TGGCTATATGTTTAT-3′; Spike1RPSL1F, 5′-AGAACCATTTTTTGG-CTCGATTGCATTGTACAATCAAGAGGCGGCGGAGGCGGCCTGG-TGATGATGGCGGGA-3′; Spike1RPSL123R, 5′-AAAGCGGAACA-ACTGCCCAAGCAAAAGACTCTCGGTAAGGTTACCAATGCTTAA-TCAGTGA-3′; Spike-DHR1-RPSLF, 5′-GGTCTCTCTTCCTGCCAC-ATGGACGCCATCACATCATCTGGGCCTGGTGATGATGGCGGGA-3′; Spike-DHR1, 5′-RPSLRATGTCTATCATACTCTAGACAGAAAT-CCCTGACACGTTCGTTACCAATGCTTAATCAGTGA-3′; Spike1R-PSL4F, 5′-CGCTCTGAGAAATGAGCTAGAGGAGCCTCGTAGCTC-GGATAGGCCTGGTGATGATGGCGGGA-3′; Spike1RPSL4R, 5′-TG-CACTGCAACACTTCCTTGGAGAATCCTCTGCAGACTTTTTACCA-ATGCTTAATCAGTGA-3′; SpikeTest123F, 5′-TTTACCTGCTTATGAA-CCAGC-3′; SpikeTest123R, 5′-CTATGAAAAATGTTCCACACC-3′; Spike-DHR1-TestR, 5′-TATGAAACAGTCACATGGGCAG-3′; Spike-c-terminus-TestF, 5′-TGTGCTATCTGCAAATTACTGC-3′; and Spike-c-terminus-TestR, 5′-AATTCCTGATCTTCTTCTCCG-3′.

SPK1 protein expression in *Escherichia coli* and live-cell imaging of N-terminal fragments

SPK1 fragments were amplified from the full-length cDNA clone of SPK1 in pBSK-SPK1 (Qiu et al., 2002), cloned into the pENTR/D-Topo cloning vector (Invitrogen, K240020) and confirmed by sequencing. The resulting pENTR clones were then recombined into either the recombinant protein expression vector pDEST17 (Invitrogen, 11803-012) and/or the binary destination vector pGWB6 (a gift from Tsuyoshi Nakagawa, Research Institute of Molecular Genetics, Shimane University, Japan) for plant transformation and live-cell imaging. The SPKN1 fragment spanned amino acids 1-995 and was amplified using SPKN1(1-995)F (5′-CACCCATATG-GAGAACAACAATCTTGGT-3′) and SPKN1(1-995)R (5′-GTCGACAT-TACGAACAATTTGCAGCA-3′), and used to generate pGWB6-SPKN995 (N-terminal GFP tag). The SPK1N2 fragment spanned amino acids 1-286 and was amplified with SPKN2F (5′-CACCGAATTCATGGAGAACAA-CAATCTTGGTCTT-3′) and SPKN2R (5′-GTCGACAGTGTTTGTGGT-GAGATTAT-3′) to generate pGWB6-SPKN2. The SPK1N3 fragment spanned amino acids 136-286 and was amplified with SPKN3F (5′-CACCGAATTCGGTCAGAGAACTCCTGAATCTCCT-3′) and SPKN2R (5′-GTCGACAGTGTTTGTGGTGAGATTAT-3′) to generate pDEST17-SPKN3 and pGWB6-SPKN3. The SPK1N4 fragment spanned amino acids 136-312 and was amplified using SPKN3F (5′-CACCGAATTCGGTCA-GAGAACTCCTGAATCTCCT-3′) and SPKN4R (5′-GTCGACTGGTT-CATAAACACCATCAT-3′) to generate pGWB6-SPKN4. The 6xHis SPKN, 6xHis SPKN3 and 6xHis AnnexinV proteins for lipid-binding analysis were expressed by freshly transforming the plasmids into *E. coli* strain BL21 (DE3) *E. coli* (Novagen, Madison, WI, USA) or Rosetta *E. coli*, and induced with 0.2 mM isopropyl β-D-thiogalactoside (Gold Biotechnology, St Louis, MO, USA) at OD_{600} of 0.6 to 0.7, and then grown at 16°C for 16 h (SPKN and SPKN3) or 3 h at 28°C (AnnexinV). Soluble proteins were purified by using Ni-NTA His-Bind resin (Novagen) according to the manufacturer's specifications. Proteins were then dialyzed into 20 mM Tris (pH 7.5) and 10% glycerol, and then concentrated using standard centrifugal devices. Protein concentrations were determined by running the purified proteins on an SDS-PAGE gel along with known amounts of dilutions of BSA, and then comparing the densitometry readings of Coomassie Brilliant Blue-stained bands.

Live-cell imaging

YFP:SPK1 deletion constructs were imaged using a spinning disk confocal microscope. Fluorescent images were detected using a Photometrix Evolve 512 (Tucson, Az) intensified CCD camera acquired using a CSU-X1 spinning disk confocal head (Yokogawa Electric Corporation, Tokyo, Japan) mounted on a Zeiss Observer.Z1 inverted microscope with a 60×

C-Apo 1.2 NA water-immersion objective or a 100× PlanApo 1.46 NA oil-immersion objective to quantify individual punctae. Image processing and quantification were performed using ImageJ (http://imagej.nih.gov/ij/) and SlideBook version 6.0 (Intelligent Imaging Innovations, Denver, CO, USA). Images were edited using Photoshop CS5 (Adobe) for data presentation. Fluorescent images of SPK1 N-terminal fragments were acquired using a Zeiss LSM780 inverted microscope with a 40× C-Apo 1.1 NA water-immersion objective lens. GFP was excited by a 488 nm laser line with 12% and 15% laser power for free GFP and GFP-SPKNs, respectively, and with the scan speed of 3.15 µsec/pixel. Images were captured in the 493-598-nm emission window. To inhibit PI-3 kinase, 2-µl drops of 50 µM wortmannin (Sigma-Aldrich, W1628) were applied on the shoot meristem and emerging leaves of ten to 13 DAG seedlings expressing YFP:SPK1 or 2xFYVE: YFP (a gift from T. Munnik, Amsterdam, The Netherlands; Vermeer et al. 2006). The peroxisomal marker CFP:PTS1 (Nelson et al., 2007) was obtained from the *Arabidopsis* Biological Resource Center, and was excited with a 440 nm laser and detected with a 450-475 nm bandpass filter. Trichome images were acquired using a chambered glass slide. In wash-out experiments, seedlings were removed from the slide, rinsed with DMSO-containing buffer twice and then incubated in DMSO-containing buffer for 1 h prior to remounting on the chambered slide. The various YFP:SPK1 proteins analyzed were scored as having 'punctate' localization if there were five or more particles detected. They were classified as having tip localization if signal was clustered at the extreme apex of a branch. SPK1 localizations were classified as 'cortical' if a clear majority (70% or more) of punctae were within the same image plane as the plasma membrane or one optical section inward. SPK1 localization was classified as subcortical if a clear majority (70% or more) of punctae present were two or more image planes interior to the plasma membrane. 'Mixed' localization was defined as cells having numerous punctae at cortical and subcortical locations.

Plant transformation and rescue construct phenotyping

For YFP:SPK1 deletion construct analysis in the spk1-1 null background, the constructs were transformed into kanamycin-resistant SPK1-1/*spk1-1* heterozygous plants (the *spk1-1* T-DNA allele harbors kanamycin resistance), because of the sterility of spk1 homozygous lines. Transformation was performed using the floral dip *Agrobacterium*-mediated transformation method (Clough and Bent, 1998). T1 seeds were screened for Basta resistance on 1/2× MS plates containing 1:50,000 (10 µg/ml) Basta, and screened on a spinning disk microscope for YFP signal. Transformants with YFP signal were selfed and seed was bulked for further analysis. Because *spk1-1/spk1-1* plants could not be transformed and progeny observed for rescue, determination of phenotypic rescue activity was based on χ^2 analyses of phenotypic scoring of the *spk1-1* phenotype of T2 plants on MS Basta plates, with the null hypothesis being that the transgene does not rescue. One would expect a 3:1 SPK1 to *spk1-1* phenotype segregation in this case. To test for partial transgene function, ΔDHR3 and ΔDHR1 constructs were transformed into *spk1-666*. Transformants with YFP signal were analyzed for phenotype, self fertilized and bulked for further analyses. Lack of rescue activity was determined by analyzing *spk1-666* trichome phenotype in Basta-resistant plants. In cases in which no T1 plants were obtained in the *SPK1*/*spk1-1* background, the constructs were crossed from the *spk1-666* or wild-type plants, and then crossed into the *spk1-1* background.

Whole-plant protein extraction and western blotting

Segregating progeny of YFP:SPK1 deletion construct plant lines that had a *spk1-1/spk1-1* phenotype with fluorescent signal were chosen for protein extraction and western blotting to demonstrate the size of the fluorescent constructs. Protein extractions from plants were performed by grinding ∼70 mg of plant tissue (usually two plants) in liquid nitrogen, resuspending in two volumes of 2× Laemmli solution [80 mM Tris (pH 6.8), 8% SDS, 0.046 mM Bromophenol Blue, 6.66 mM EDTA, 200 mM DTT and 20% glycerol, Sigma-Aldrich) that also contained protease inhibitors and PMSF, and then boiling for 10 min. Plant protein extracts isolated from expanded leaves of *spk1*-1 $Basta_R$ plants that were segregating for the SPK1 deletion constructs were loaded in parallel with wild type and separated on 7.5% SDS-PAGE gels using a Bio-Rad Mini-Protein3 Cell (Hercules, CA, USA) and transferred to 0.2 µm reinforced nitrocellulose membranes (Whatman Optitran BA-S 83, Dassel, Germany) in chilled 25 mM Tris, 192 mM glycine, 20% (v/v) methanol and 0.1% SDS buffer using a Bio-Rad Mini Trans-Blot Electrophoretic transfer cell (Hercules) for 2 h at 80 V. Membranes were rinsed briefly with TTBS and then blocked in 5% dry milk in TTBS for 1 h at room temperature. Primary antibodies were incubated overnight at 4°C [1:1000 anti-SPKN (Basu et al., 2008); and 1:20,000 anti-Pep carboxylase (Rockland Immunochemicals, Gilbertsville, PA, USA)], washed three times for 10 min at room temperature with chilled TTBS, and then incubated with an HRP-conjugated goat-anti-rabbit IgG secondary antibody (Pierce, Rockford, IL, USA) at 1:50,000 for 1-2 h. Washing after secondary antibody incubation was performed in the same way as with primary antibodies. Signal was detected on X-ray film with SuperSignal West Pico Chemiluminescent Substrate (Pierce).

AlphaFold and RoseTTAFold three-dimensional models for SPK1 and structural comparisons

An existing AlphaFold model of protein structure prediction for SPK1 (Q8SAB7) was downloaded from the AlphaFold Protein Structure Database (www.alphafold.ebi.ac.uk/), last updated on July 1, 2021 with AlphaFold v2.0. In the Robetta website (https://robetta.bakerlab.org/), SPK1 sequences between amino acid residues 1 to 1117, due to its limitation for searching, were used for structure prediction using the RoseTTAFold method on September 4, 2021. The AlphaFold SPK1 model was exported as PDB format files containing a full-length protein, truncated DHR3 domain, truncated DHR3 domain with additional two β-strands (residues 330–334 and 362–371), and amino acid residues from 136 to 371 (the start of DHR1 to the end of addition two β-strands). Subsequently, all these protein structures were queried against the PDB25 subset, last updated on September 19, 2021. All Dali searches for structural similarity comparisons with experimentally determined proteins were performed at the Dali server (http://ekhidna2.biocenter.helsinki.fi/dali/). Surface electrostatic potentials were calculated using the Adaptive Poisson-Boltzmann Solver plug-in on PyMOL2. Then, the inferred electrostatic potentials were visualized on the surface of the AlphaFold SPK1 model using PyMOL2.

Acknowledgements

This paper is dedicated to the work of Chunhua Zhang who discovered the lipid-binding activities of SPIKE1 during her PhD thesis research in the Szymanski lab. Chunhua passed away on May 15, 2021 (https://blog.aspb.org/tribute-chunhua-zhang/). We thank the *Arabidopsis* Biological Resource Center (Columbus, OH, USA) for providing *rdr6-11* (CS24285) and CFP:PTS1.

Competing interests

The authors declare no competing or financial interests.

Author contributions

Conceptualization: M.Y., C.Z., D.B.S.; Methodology: E.L.M., M.Y., C.Z., Y.L., L.M.R., J.M.A., D.B.S.; Validation: E.L.M., M.Y., C.Z., Y.L., L.M.R.; Formal analysis: E.L.M., Y.L.; Investigation: E.L.M., M.Y., C.Z., Y.L., L.M.R., D.B.S.; Resources: J.M.A., D.B.S.; Data curation: E.L.M., M.Y., C.Z., Y.L., L.M.R., J.M.A., D.B.S.; Writing - original draft: E.L.M., M.Y., Y.L., D.B.S.; Writing - review & editing: E.L.M., M.Y., Y.L., L.M.R., J.M.A., D.B.S.; Visualization: E.L.M., M.Y., C.Z., Y.L., D.B.S.; Supervision: J.M.A., D.B.S.; Project administration: J.M.A., D.B.S.; Funding acquisition: J.M.A., D.B.S.

Funding

This work was supported by grants from the National Science Foundation (1715544 and 1121893 to D.B.S.).

References

Baek, M., DiMaio, F., Anishchenko, I., Dauparas, J., Ovchinnikov, S., Lee, G. R., Wang, J., Cong, Q., Kinch, L. N., Schaeffer, R. D. et al. (2021). Accurate prediction of protein structures and interactions using a three-track neural network. *Science* **373**, 871. doi:10.1126/science.abj8754

Bascom, C., Jr, Burkart, G. M., Mallett, D. R., O'Sullivan, J. E., Tomaszewski, A. J., Walsh, K. and Bezanilla, M. (2019). Systematic survey of the function of ROP regulators and effectors during tip growth in the moss Physcomitrella patens. *J. Exp. Bot.* **70**, 447-457. doi:10.1093/jxb/ery376

Basu, D., Le, J., Zakharova, T., Mallery, E. L. and Szymanski, D. B. (2008). A SPIKE1 signaling complex controls actin-dependent cell morphogenesis through

the heteromeric WAVE and ARP2/3 complexes. *Proc. Natl. Acad. Sci. USA* **105**, 4044-4049. doi:10.1073/pnas.0710294105

Berken, A. and Wittinghofer, A. (2008). Structure and function of Rho-type molecular switches in plants. *Plant Physiol. Biochem.* **46**, 380-393. doi:10.1016/j.plaphy.2007.12.008

Chang, L. F., Yang, J., Jo, C. H., Boland, A., Zhang, Z. G., McLaughlin, S. H., Abu-Thuraia, A., Killoran, R. C., Smith, M. J., Cote, J.-F. et al. (2020). Structure of the DOCK2-ELMO1 complex provides insights into regulation of the auto-inhibited state. *Nat. Commun.* **11**, 3464. doi:10.1038/s41467-020-17271-9

Chen, R.-H., CorbalanGarcia, S. and BarSagi, D. (1997). The role of the PH domain in the signal-dependent membrane targeting of Sos. *EMBO J.* **16**, 1351-1359. doi:10.1093/emboj/16.6.1351

Chiou, J.-G., Balasubramanian, M. K. and Lew, D. J. (2017). Cell polarity in yeast. *Annu. Rev. Cell Dev. Biol.* **33**, 77-101. doi:10.1146/annurev-cellbio-100616-060856

Chung, J., Torta, F., Masai, K., Lucast, L., Czapla, H., Tanner, L. B., Narayanaswamy, P., Wenk, M. R., Nakatsu, F. and De Camilli, P. (2015). PI4P/phosphatidylserine countertransport at ORP5- and ORP8-mediated ER-plasma membrane contacts. *Science* **349**, 428-432. doi:10.1126/science.aab1370

Clough, S. and Bent, A. (1998). Floral dip: a simplified method for Agrobacterium-mediated transformation of *Arbidopsis thaliana*. *Plant J.* **16**, 735-743. doi:10.1046/j.1365-313x.1998.00343.x

Corbalan-Garcia, S. and Gomez-Fernandez, J. C. (2014). Signaling through C2 domains: more than one lipid target. *Biochim. Biomembr. Acta Biomembr.* **1838**, 1536-1547. doi:10.1016/j.bbamem.2014.01.008

Cote, J.-F. and Vuori, K. (2002). Identification of an evolutionarily conserved superfamily of DOCK180-related proteins with guanine nucleotide exchange activity. *J. Cell Sci.* **115**, 4901-4913. doi:10.1242/jcs.00219

Cote, J.-F., Motoyama, A. B., Bush, J. A. and Vuori, K. (2005). A novel and evolutionarily conserved PtdIns(3,4,5)P3-binding domain is necessary for DOCK180 signaling. *Nat. Cell Biol.* **7**, 797-807. doi:10.1038/ncb1280

Denninger, P., Reichelt, A., Schmidt, V. A. F., Mehlhorn, D. G., Asseck, L. Y., Stanley, C. E., Keinath, N. F., Evers, J.-F., Grefen, C. and Grossmann, G. (2019). Distinct RopGEFs successively drive polarization and outgrowth of root hairs. *Curr. Biol.* **29**, 1854-1865.e55. doi:10.1016/j.cub.2019.04.059

Duan, Q., Kita, D., Li, C., Cheung, A. Y. and Wu, H.-M. (2010). FERONIA receptor-like kinase regulates RHO GTPase signaling of root hair development. *Proc. Natl. Acad. Sci. USA.* **107**, 17821-17826. doi:10.1073/pnas.1005366107

Etienne-Manneville, S. and Hall, A. (2002). Rho GTPases in cell biology. *Nature* **420**, 629-635. doi:10.1038/nature01148

Feiguelman, G., Fu, Y. and Yalovsky, S. (2018). ROP GTPases structure-function and signaling pathways. *Plant Physiol.* **176**, 57-79. doi:10.1104/pp.17.01415

Gumienny, T. L., Brugnera, E., Tosello-Trampont, A.-C., Kinchen, J. M., Haney, L. B., Nishiwaki, K., Walk, S. F., Nemergut, M. E., Macara, I. G., Francis, R. et al. (2001). CED-12/ELMO, a novel member of the CrkII/Dock180/rac pathway, is required for phagocytosis and cell migration. *Cell* **107**, 27-41. doi:10.1016/S0092-8674(01)00520-7

Hasegawa, H., Kiyokawa, E., Tanaka, S., Nagashima, K., Gotoh, N., Shibuya, M., Kurata, T. and Matsuda, M. (1996). DOCK180, a major CRK-binding protein, alters cell morphology upon translocation to the cell membrane. *Mol. Cell. Biol.* **16**, 1770-1776. doi:10.1128/MCB.16.4.1770

Hurley, J. H. and Misra, S. (2000). Signaling and subcellular targeting by membrane-binding domains. *Annu. Rev. Biophys. Biomol. Struct.* **29**, 49-79. doi:10.1146/annurev.biophys.29.1.49

Jimenez-Sanchez, A. (2016). Coevolution of RAC Small GTPases and their regulators GEF proteins. *Evol. Bioinform.* **12**, 121-131. doi:10.4137/EBO.S38031

Jumper, J., Evans, R., Pritzel, A., Green, T., Figurnov, M., Ronneberger, O., Tunyasuvunakool, K., Bates, R., Zidek, A., Potapenko, A. et al. (2021). Highly accurate protein structure prediction with AlphaFold. *Nature* **596**, 583-589. doi:10.1038/s41586-021-03819-2

Kaothien, P., Ok, S. H., Shuai, B., Wengier, D., Cotter, R., Kelley, D., Kiriakopolos, S., Muschietti, J. and McCormick, S. (2005). Kinase partner protein interacts with the LePRK1 and LePRK2 receptor kinases and plays a role in polarized pollen tube growth. *Plant J.* **42**, 492-503. doi:10.1111/j.1365-313X.2005.02388.x

Karlovich, C. A., Bonfini, L., Mccollam, L., Rogge, R. D., Daga, A., Czech, M. P. and Banerjee, U. (1995). In vivo functional analysis of the Ras exchange factor son of sevenless. *Science* **268**, 576-579. doi:10.1126/science.7725106

Kost, B. (2008). Spatial control of Rho (Rac-Rop) signaling in tip-growing plant cells. *Trends Cell Biol.* **18**, 119-127. doi:10.1016/j.tcb.2008.01.003

Kotchoni, S. O., Zakharova, T., Mallery, E. L., Le, J., El-Assal, S. E.-D. and Szymanski, D. B. (2009). The association of the Arabidopsis actin-related protein (ARP) 2/3 complex with cell membranes is linked to its assembly status, but not its activation. *Plant Physiol.* **151**, 2095-2109. doi:10.1104/pp.109.143859

Kozubowski, L., Saito, K., Johnson, J. M., Howell, A. S., Zyla, T. R. and Lew, D. J. (2008). Symmetry-breaking polarization driven by a Cdc42p GEF-PAK complex. *Curr. Biol.* **18**, 1719-1726. doi:10.1016/j.cub.2008.09.060

Kukimoto-Niino, M., Katsura, K., Kaushik, R., Ehara, H., Yokoyama, T., Uchikubo-Kamo, T., Nakagawa, R., Mishima-Tsumagari, C., Yonemochi, M., Ikeda, M. et al. (2021). Cryo-EM structure of the human ELMO1-DOCK5-Rac1 complex. *Sci. Adv.* **7**, eabg3147. doi:10.1126/sciadv.abg3147

Kumar, S., Stecher, G., Suleski, M. and Hedges, S. B. (2017). TimeTree: a resource for timelines, timetrees, and divergence times. *Mol. Biol. Evol.* **34**, 1812-1819. doi:10.1093/molbev/msx116

Liu, J., Liu, M. X., Qiu, L. P. and Xie, F. (2020). SPIKE1 activates the GTPase ROP6 to guide the polarized growth of infection threads in Lotus japonicus. *Plant Cell.* **32**, 3774-3791. doi:10.1105/tpc.20.00109

Meca, J., Massoni-Laporte, A., Martinez, D., Sartorel, E., Loquet, A., Habenstein, B. and McCusker, D. (2019). Avidity-driven polarity establishment via multivalent lipid-GTPase module interactions. *EMBO J.* **38**, e99652. doi:10.15252/embj.201899652

Meller, N., Merlot, S. and Guda, C. (2005). CZH proteins: a new family of Rho-GEFs. *J. Cell Sci.* **118**, 4937-4946. doi:10.1242/jcs.02671

Miyamoto, Y., Yamauchi, J., Sanbe, A. and Tanoue, A. (2007). Dock6, a Dock-C subfamily guanine nucleotide exchanger, has the dual specificity for Rac1 and Cdc42 and regulates neurite outgrowth. *Exp. Cell Res.* **313**, 791-804. doi:10.1016/j.yexcr.2006.11.017

Moser von Filseck, J., Copic, A., Delfosse, V., Vanni, S., Jackson, C. L., Bourguet, W. and Drin, G. (2015). Phosphatidylserine transport by ORP/Osh proteins is driven by phosphatidylinositol 4-phosphate. *Science* **349**, 432-436. doi:10.1126/science.aab1346

Namekata, K., Harada, C., Taya, C., Guo, X., Kimura, H., Parada, L. F. and Harada, T. (2010). Dock3 induces axonal outgrowth by stimulating membrane recruitment of the WAVE complex. *Proc. Natl. Acad. Sci. USA* **107**, 7586-7591. doi:10.1073/pnas.0914514107

Nelson, B. K., Cai, X. and Nebenfuhr, A. (2007). A multicolored set of *in vivo* organelle markers for co-localization studies in Arabidopsis and other plants. *Plant J.* **51**, 1126-1136. doi:10.1111/j.1365-313X.2007.03212.x

Nishikimi, A., Fukuhara, H., Su, W., Hongu, T., Takasuga, S., Mihara, H., Cao, Q., Sanematsu, F., Kanai, M., Hasegawa, H. et al. (2009). Sequential regulation of DOCK2 dynamics by two phospholipids during neutrophil chemotaxis. *Science* **324**, 384-387. doi:10.1126/science.1170179

Nolan, K. M., Barrett, K., Lu, Y., Hu, K.-Q., Vincent, S. and Settleman, J. (1998). Myoblast city, the *Drosophila* homolog of DOCK180/CED-5, is required in a rac signaling pathway utilized for multiple developmental processes. *Genes Dev.* **12**, 3337-3342. doi:10.1101/gad.12.21.3337

Oda, Y. and Fukuda, H. (2012). Initiation of cell wall pattern by a Rho- and microtubule-driven symmetry breaking. *Science* **337**, 1333-1336. doi:10.1126/science.1222597

Platre, M. P., Bayle, V., Armengot, L., Bareille, J., Marques-Bueno, M. D. M., Creff, A., Maneta-Peyret, L., Fiche, J.-B., Nollmann, M., Miege, C. et al. (2019). Developmental control of plant Rho GTPase nano-organization by the lipid phosphatidylserine. *Science* **364**, 57-62. doi:10.1126/science.aav9959

Premkumar, L., Bobkov, A. A., Patel, M., Jaroszewski, L., Bankston, L. A., Stec, B., Vuori, K., Cote, J.-F. and Liddington, R. C. (2010). Structural basis of membrane targeting by the Dock180 family of Rho family guanine exchange factors (Rho-GEFs). *J. Biol. Chem.* **285**, 13211-13222. doi:10.1074/jbc.M110.102517

Qiu, J.-L., Jilk, R., Marks, M. D. and Szymanski, D. B. (2002). The *Arabidopsis SPIKE1* gene is required for normal cell shape control and tissue development. *Plant Cell.* **14**, 101-118. doi:10.1105/tpc.010346

Ren, H., Dang, X., Yang, Y., Huang, D., Liu, M., Gao, X. and Lin, D. (2016). SPIKE1 activates ROP GTPase to modulate petal growth and shape. *Plant Physiol.* **172**, 358-371. doi:10.1104/pp.16.00788

Rossman, K. L., Der, C. J. and Sondek, J. (2005). GEF means go: Turning on RHO GTPases with guanine nucleotide-exchange factors. *Nat. Rev. Mol. Cell Biol.* **6**, 167-180. doi:10.1038/nrm1587

Ryan, J. M. and Nebenfuhr, A. (2018). Update on myosin motors: molecular mechanisms and physiological functions. *Plant Physiol.* **176**, 119-127. doi:10.1104/pp.17.01429

Sakurai, T., Kukimoto-Niino, M., Kunimura, K., Yamane, N., Sakata, D., Aihara, R., Yasuda, T, Yokoyama, S., Shirouzu, M., Fukui Y. et al. (2021). DOCK8 links PI(4,5)P2 signal to Cdc42 activation. *Life Sci. Alliance* **4**, e202000873; doi:10.26508/lsa.202000873

Sanematsu, F., Nishikimi, A., Watanabe, M., Hongu, T., Tanaka, Y., Kanaho, Y., Cote, J.-F. and Fukui, Y. (2013). Phosphatidic acid-dependent recruitment and function of the Rac activator DOCK1 during dorsal ruffle formation. *J. Biol. Chem.* **288**, 8092-8100. doi:10.1074/jbc.M112.410423

Schmidt, A. and Hall, A. (2002). Guanine nucleotide exchange factors for Rho GTPases: turning on the switch. *Genes Dev.* **16**, 1587-1609. doi:10.1101/gad.1003302

Shichrur, K. and Yalovsky, S. (2006). Turning ON the switch–RhoGEFs in plants. *Trends Plant Sci.* **11**, 57-59. doi:10.1016/j.tplants.2005.12.001

Thompson, A. P., Bitsina, C., Gray, J. L., von Delft, F. and Brennan, P. E. (2021). RHO to the DOCK for GDP disembarking: Structural insights into the DOCK GTPase nucleotide exchange factors. *J. Biol. Chem.* **296**, 100521. doi:10.1016/j.jbc.2021.100521

Uhrig, J. F., Mutondo, M., Zimmermann, I., Deeks, M. J., Machesky, L. M., Thomas, P., Uhrig, S., Rambke, C., Hussey, P. J. and Hulskamp, M. (2007). The role of Arabidopsis SCAR genes in ARP2-ARP3-dependent cell morphogenesis. *Development* **134**, 967-977. doi:10.1242/dev.02792

Vermeer, J. E. M., van Leeuwen, W., Tobena-Santamaria, R., Laxalt, A. M., Jones, D. R., Divecha, N., Gadella, T. W. J., Jr and Munnik, T. (2006). Visualization of PtdIns3*P* dynamics in living plant cells. *Plant J.* **47**, 687-700. doi:10.1111/j.1365-313X.2006.02830.x

Wang, Q., Li, Y., Ishikawa, K., Kosami, K.-I., Uno, K., Nagawa, S., Tan, L., Du, J., Shimamoto, K. and Kawano, Y. (2018). Resistance protein Pit interacts with the GEF OsSPK1 to activate OsRac1 and trigger rice immunity. *Proc. Natl. Acad. Sci. USA* **115**, E11551-E1E560. doi:10.1073/pnas.1813058115

Wu, Y.-C. and Horvitz, H. R. (1998). *C. elegans* phagocytosis and cell-migration protein CED-5 is similar to human DOCK180. *Nature* **392**, 501-504. doi:10.1038/33163

Yamauchi, J., Miyamoto, Y., Chan, J. R. and Tanoue, A. (2008). ErbB2 directly activates the exchange factor Dock7 to promote Schwann cell migration. *J. Cell Biol.* **181**, 351-365. doi:10.1083/jcb.200709033

Yanagisawa, M., Zhang, C. and Szymanski, D. B. (2013). ARP2/3-dependent growth in the plant kingdom: SCARs for life. *Front. Plant Sci.* **4**, 1-12. doi:10.3389/fpls.2013.00166

Yanagisawa, M., Desyatova, A. S., Belteton, S. A., Mallery, E. L., Turner, J. A. and Szymanski, D. B. (2015). Patterning mechanisms of cytoskeletal and cell wall systems during leaf trichome morphogenesis. *Nature Plant.* **1**, 15014. doi:10.1038/nplants.2015.14

Yanagisawa, M., Alonso, J. M. and Szymanski, D. B. (2018). Microtubule-dependent confinement of a cell signaling and actin polymerization control module regulates polarized cell growth. *Curr. Biol.* **28**, 2459-2466.e4. doi:10.1016/j.cub.2018.05.076

Yang, J., Zhang, Z., Roe, S. M., Marshall, C. J. and Barford, D. (2009). Activation of Rho GTPases by DOCK exchange factors is mediated by a nucleotide sensor. *Science* **325**, 1398-1402. doi:10.1126/science.1174468

Zhang, Y. and McCormick, S. (2007). A distinct mechanism regulating a pollen-specific guanine nucleotide exchange factor for the small GTPase Rop in Arabidopsis thaliana. *Proc. Natl. Acad. Sci. USA* **104**, 18830-18835. doi:10.1073/pnas.0705874104

Zhang, D. and Aravind, L. (2010). Identification of novel families and classification of the C2 domain superfamily elucidate the origin and evolution of membrane targeting activities in eukaryotes. *Gene* **469**, 18-30. doi:10.1016/j.gene.2010.08.006

Zhang, C., Kotchoni, S. O., Samuels, A. L. and Szymanski, D. B. (2010). SPIKE1 signals originate from and assemble specialized domains of the endoplasmic reticulum. *Curr. Biol.* **20**, 2144-2149. doi:10.1016/j.cub.2010.11.016

Zhang, C., Mallery, E., Reagan, S., Boyko, V. P., Kotchoni, S. O. and Szymanski, D. B. (2013). The endoplasmic reticulum is a reservoir for WAVE/SCAR regulatory complex signaling in the Arabidopsis leaf. *Plant Physiol.* **162**, 689-706. doi:10.1104/pp.113.217422

Zheng, Y., Zangrilli, D., Cerione, R. A. and Eva, A. (1996). The pleckstrin homology domain mediates transformation by oncogenic Dbl through specific intracellular targeting. *J. Biol. Chem.* **271**, 19017-19020. doi:10.1074/jbc.271.32.19017

Zhou, R., Benavente, L. M., Stepanova, A. N. and Alonso, J. M. (2011). A recombineering-based gene tagging system for Arabidopsis. *Plant J.* **66**, 712-723. doi:10.1111/j.1365-313X.2011.04524.x

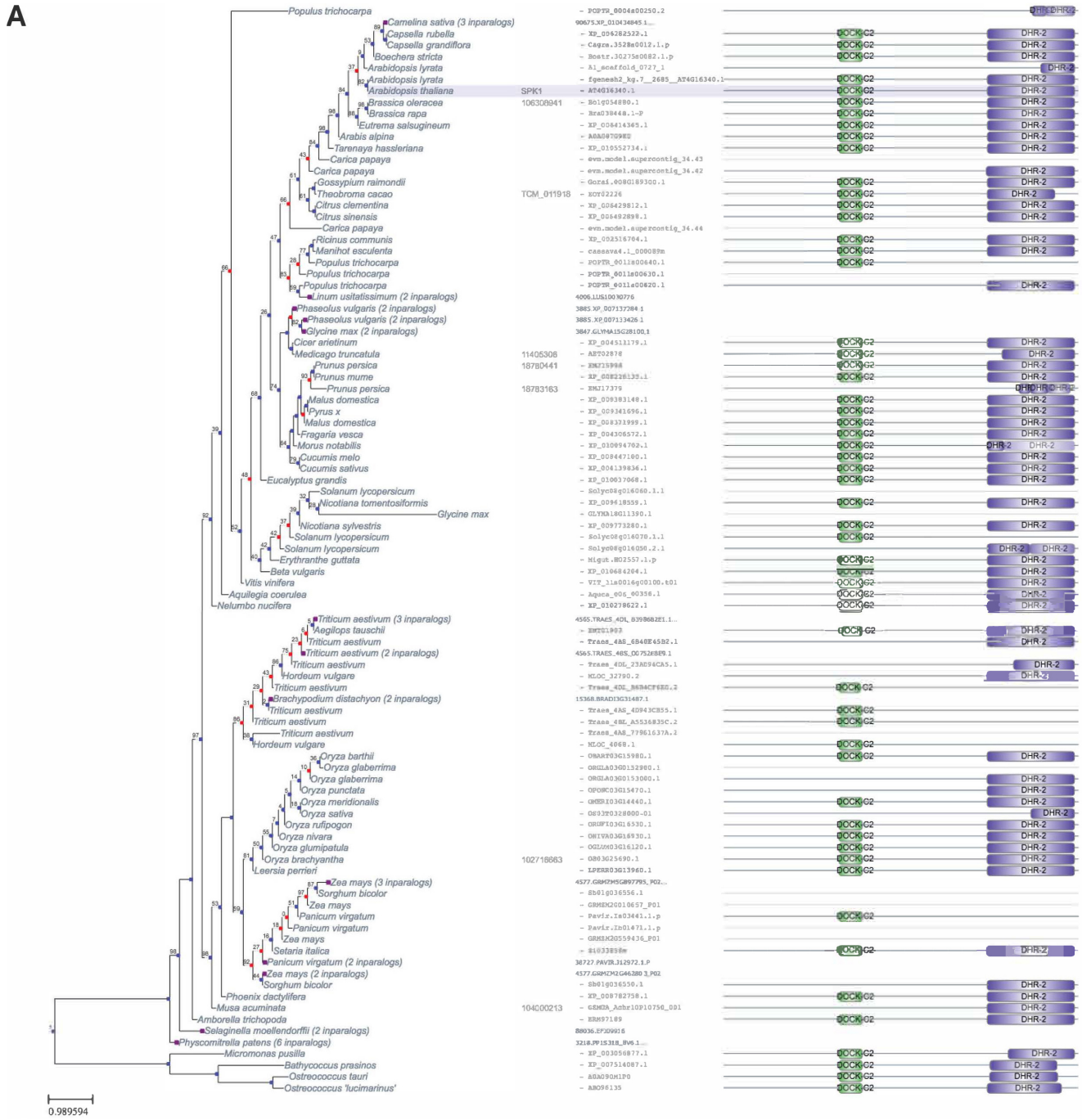

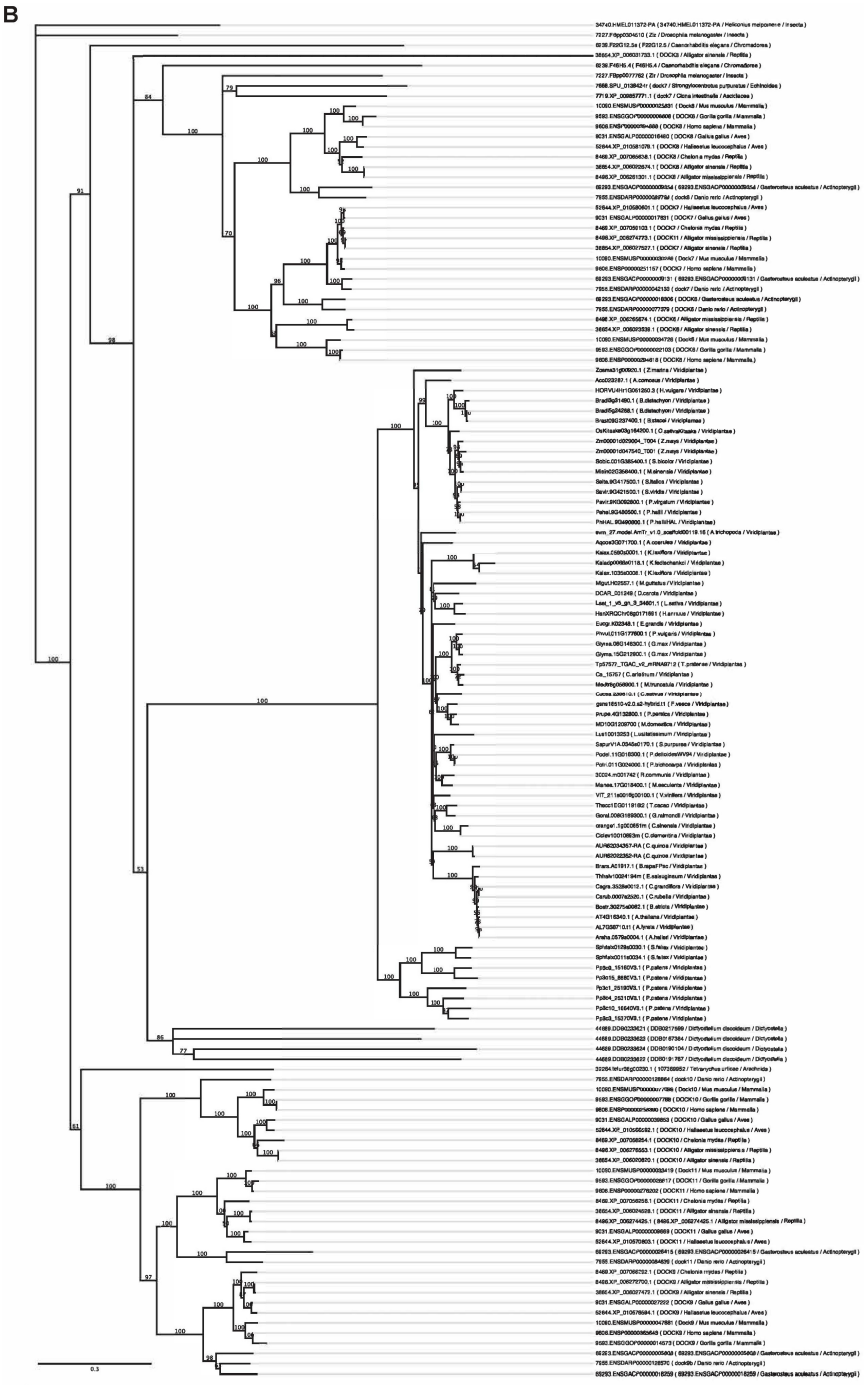

Fig S1. Phylogeny of SPK1 orthologs in the plant and animal kingdoms.

(A) Phylogeny and domain organization of SPK1 orthologs. Plant orthologs to Arabidopsis SPK1 were obtained from EggNOG (http://eggnog5.embl.de) database and searched against Pfam database (http://pfam.xfam.org). Locus IDs of SPK1 orthologs are provided in the tree. Pfam domain organizations are shown next to the phylogenetic tree.

(B) Phylogenetic analysis of plant and metazoan orthologs to Arabidopsis SPK1. Sequences from plant and animal kingdoms were obtained from Phytozome 13 (https://phytozome-next.jgi.doe.gov) and EggNOG (http://eggnog5.embl.de) databases, respectively. Geneious tree builder on Geneious Prime software (version 2021.2.2) was utilized to build the phylogenetic tree based on the multiple sequences alignment result from Cluster Omega. The numbers on the tree are the bootstrap values for clades. The scale bar indicates patristic distances.

(C) YFP:SPK rescue constructs with deletions of the DHR3 or DHR1 domains do not rescue spk1-666 trichome phenotypes. All panels except Col are in spk1-666 background. Whole plant images have scale bars of 5 mm and magntified views of representative trichomes have scale bars of 0.5 mm.

(D) SPK1 mutant proteins of the predicted size accumulate in transgenic lines. Western blots of leaf extracts probed with the anti-SPK1 antibody (upper) or PEP-C (lower) as a loading control. Col indicates wild type plants; all other extracts are from *spk1* plants, and the identity of the SPK1 construct present in *spk1* plants is indicated above each lane. The locations of the molecular weight standards are labeled to the left of the blots. 3xYPET:SPIKE1, 290 kDa; ΔDHR3, 273 kDa; ΔDHR1, 262 kDa; ΔDHR3_ΔDHR1, 245 kDa; ΔDHR2, 271 kDa.

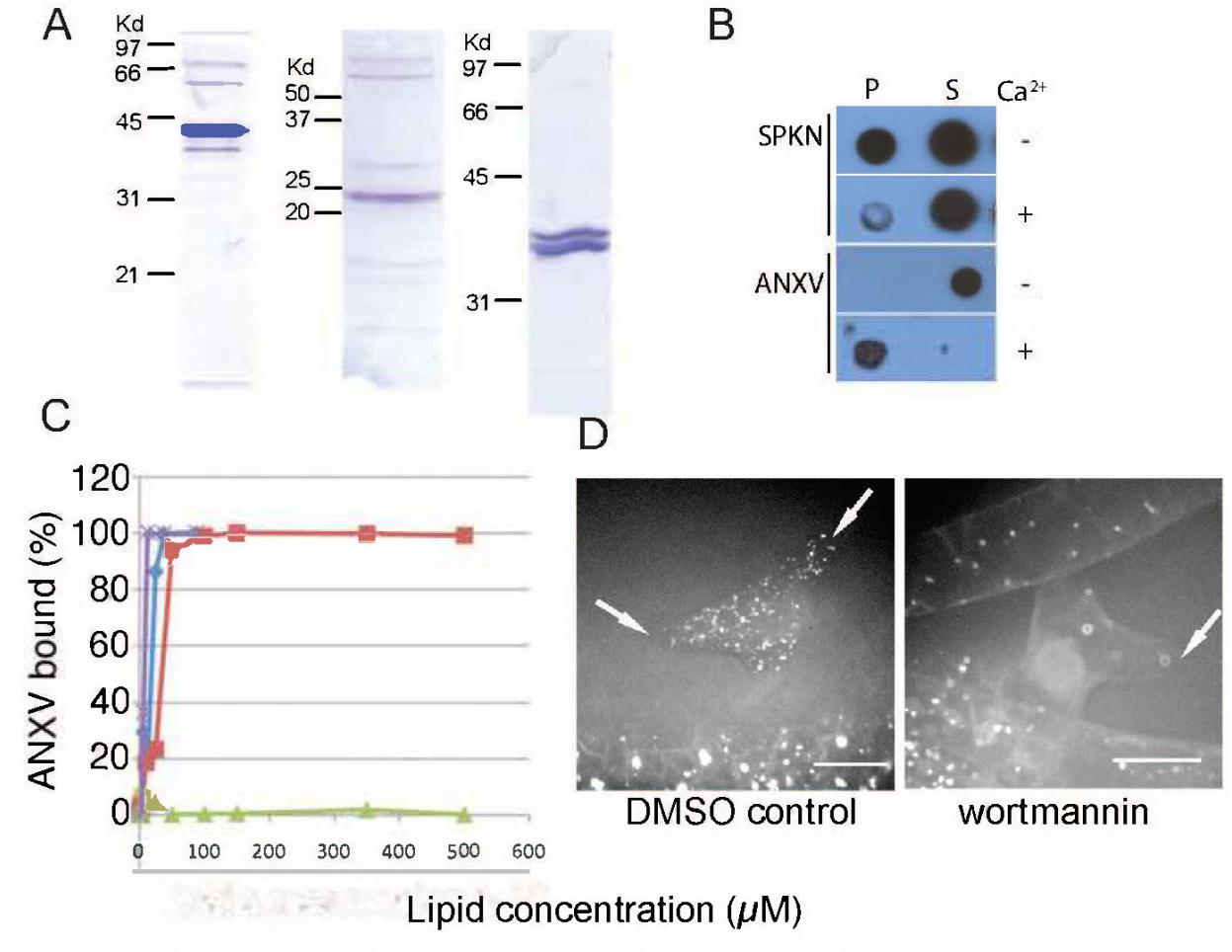

Fig. S2. Supplemental data characterizing the lipid binding selectivity of SPK1 and its wortmannin-dependence.

(A) SDS-PAGE gels of partially purified proteins. SPK N1:6xHis, 37 kDa; 6xHis:SPKN3, 24.8 kDa; human AnnexinV:6xHis, 36.8 kDa.

(B) ANX5, but not SPK1N binds to DPPS in a Ca^{2+}-dependent manner. Lipid overlay binding experiments were conducted in the presence or absence of Ca^{++}. P, pellet; S, supernatant.

(C) AnxV binds to PS without selectivity for fatty acid chain saturation. Liposome binding assays with different lipid compositions. All binding reactions conducted with the ANXV: blue, DPPS/ NTPC; purple, NTPI/NTPC; brick red, NTPS/NTPC; green, NTPC.

(D) Wortmannin reduces the number and increases the size of 2XFYVE-YFP labeled compartments in stage 4 trichomes compared to DMSO controls; arrows label trichome branch tips.

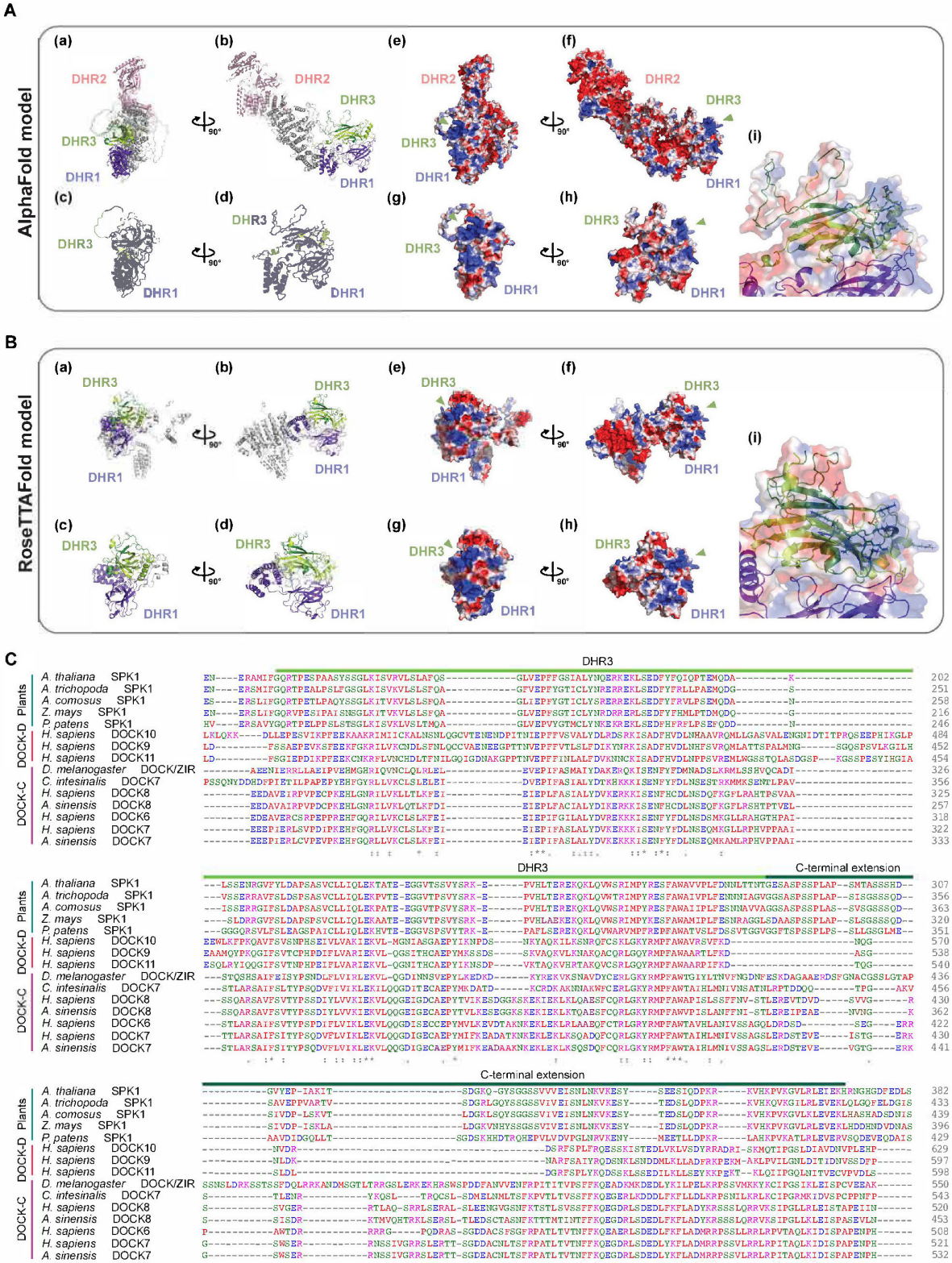

Fig. S3. Similarities of the SPK1 structure predictions using AlphaFold and RoseTTAFold.

(A & B) Overall modeled structures and domain organizations of the SPK1 predicted by AlphaFold (A) and RoseTTAFold (B). Due to length limits, the SPK1 sequence (residues 1 to 1,117) was uploaded onto the Robetta website (https://robetta.bakerlab.org/) to predict protein folding using the RoseTTAFold method on September 4, 2021. The RoseTTAFold-predicted models had a confidence level of 0.48. Two views of the full-length (a & b) and DHR3/C2 and DHR1 (c & d). The electrostatic potentials of the SPK1 models at the same orientation as (a-d) are visualized (e-h). The positively charged patch on DHR3/C2 domain is indicated with light green triangles. The zoom-in views show the basic amino acid residues on DHR3/C2 domain and with the same orientation presented in (h).

(C) The DHR3/C2 domain is conserved among SPK1 and metazoan DOCK-C and DOCK-D orthologs. The DHR3/C2 domain includes a C-terminal extension beyond the core DHR3 element defined in Fig. 1 B, as described in the results section. Clustal Omega was performed at EMBL-EBI website (https://www.ebi.ac.uk/Tools/msa/) to align SPK1 sequence to DOCKs classified as DOCK-C or DOCK-D. DHR-3 domain or the C-terminal extension were marked with the light green or the dark green bars over the sequences. Estimated conservation of amino acids was reported using "*" (a single, fully conserved residue), ":" (scoring > 0.5 in the Gonnet PAM 250 matrix), "." (≤ 0.5 and > 0) symbols.

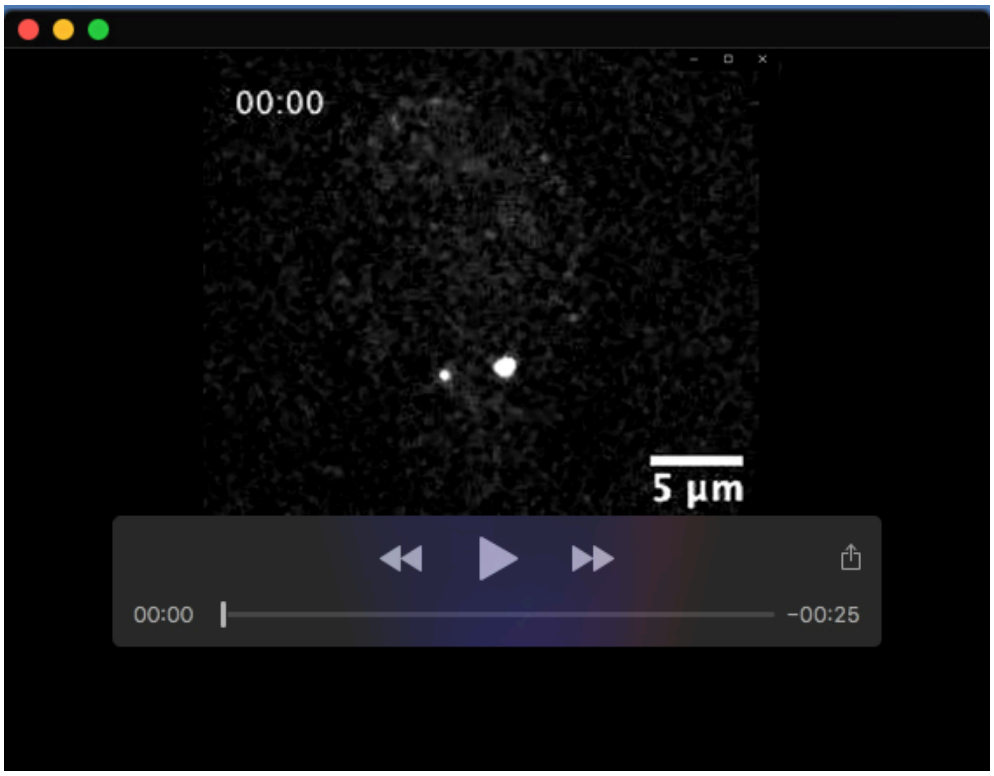

Movie 1. Time lapsed imaging of the YFP:SPK1 DHR3 deletion mutant reveals motile cytoplasmic organelles. A single image plane was acquired every 10 sec. Size bar and time stamps are labeled.